Date: May 17, 2006,   DRAFT

Electron Cooling studies for RHIC-II

I.A.1 RHIC-II parameters

This is a DRAFT of a working document.

In this document we freely use material prepared for BNL by our collaborators. In particular, by the Dubna group as part of our collaboration on the development of the BETACOOL code [1], by the Tech-X group as part of our collaboration on numerical study of the friction force with the VORPAL [2] code, and by the Fermilab electron cooling group as part of our collaboration on experimental study of the non-magnetized friction force [3].

I.A.1.1. Expected performance for heavy ions and protons

Present performance of the RHIC collider with heavy ions is limited by the process of Intra-Beam Scattering (IBS) within the beam. To achieve required luminosities for the future upgrade of the RHIC complex (known as RHIC-II) an Electron cooling system was proposed [4].

The baseline of the heavy-ion program for RHIC is operation with Au ions at total energy per beam of 100 GeV/n. For such an operation, the electron cooling should compensate IBS and provide about factor of 10 increase in average luminosity per store.

For RHIC operation with the protons, the electron cooling should assist in obtaining slightly low transverse and longitudinal emittances or prevent their significant increase due to IBS. Although, IBS is not as severe for protons as for heavy ions, a proposed increase in proton intensity for RHIC-II upgrade makes IBS one of the dominant effects as well.

Table I.A.1.1. Performance for RHIC-II

Gold at 100 GeV/n per beam	**w/o e-cooling**	**With e-cooling**
Emittance (95% norm.) [π μm]	15 $\rightarrow$ 30 (depending on the length of the store)	15 $\rightarrow$ 12
β-function in IR [m]	1.0	0.5
Number of bunches	112	112
Bunch population [10^9]	1	1
Peak luminosity [10^{26} cm^2 s^{-1}]	30	90
Average store luminosity [10^{26}]	10	50-70
Protons at 250 GeV	**w/o e-cooling**	**with e-cooling**
Emittance (95% norm.) [π μm]	20	12
β-function	1.0	0.5
Number of bunches	112	112
Bunch population [10^{11}]	2	2
Average store luminosity [10^{30}]	150	500

Without cooling:

For present operation with Au ions:

a) There is a significant emittance increase due to IBS which results in the luminosity loss. This is shown, for example, in Fig. I.A.1.1 (Run-2004 experimental data).

b) In addition, there is a significant growth of the bunch length which leads to particle loss from the bucket. Also, with such a long bunch length only central portion of the longitudinal beam distribution can effectively contribute to counts in the detector which results in an additional loss of effective luminosity.

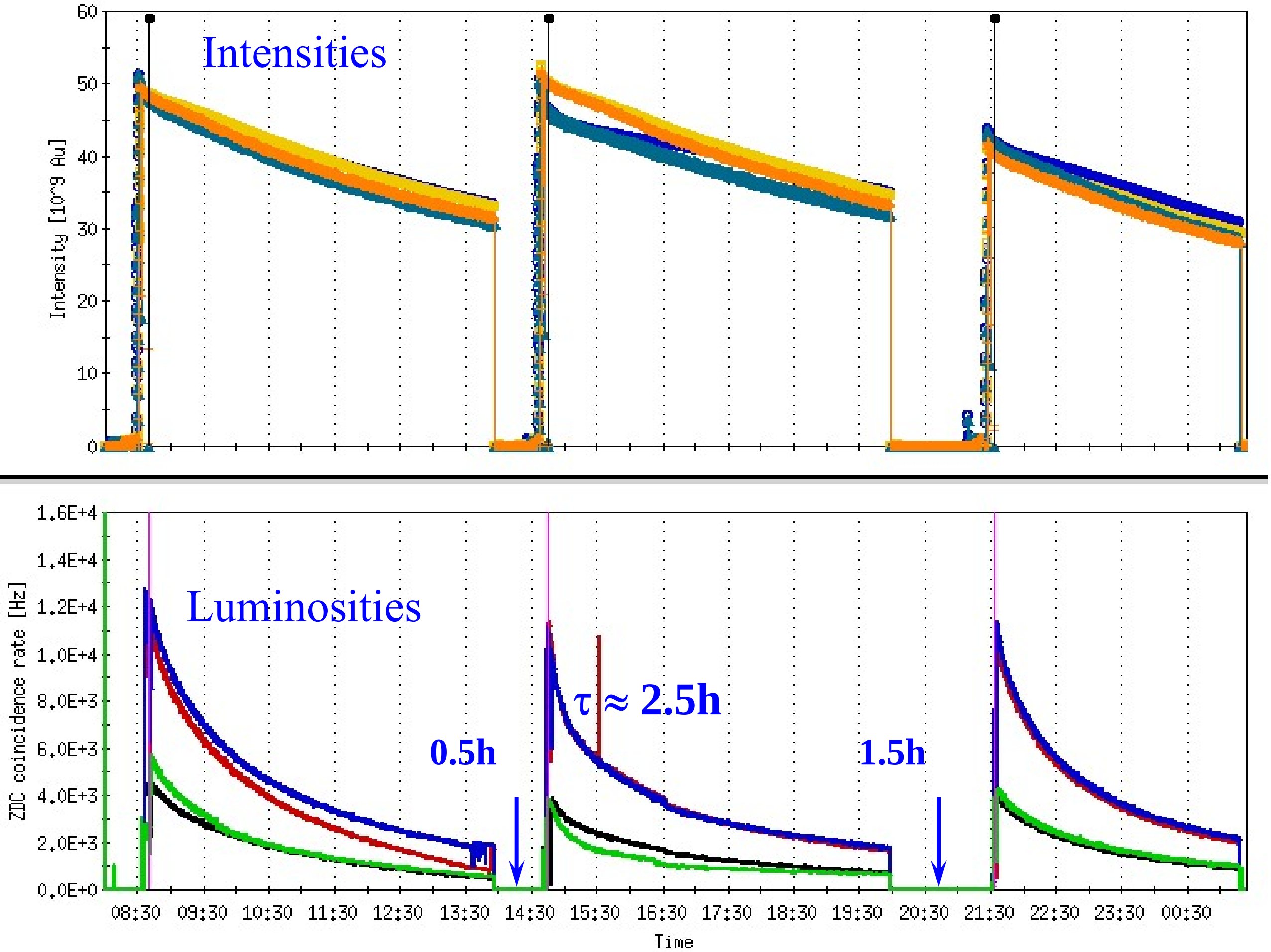

Fig. I.A.1.1 Run-2004 experiment with Au ions (40 bunches).

Note that for the enhanced luminosity of RHIC-II without cooling, the optimum length of the store is much shorter than for the present RHIC performance, shown in Fig. I.A.1.1.

With cooling:

Electron cooling of Au ions at the total beam energy of 100 GeV/n will bring into reach the desired increase of the average luminosity for the RHIC upgrade, which is about factor of 40 larger than the original design value. For the RHIC-II upgrade, electron cooling can provide about a factor of 7 increase in the luminosity of Au ions, as compared to the upgrade without cooling.

Figure 1.A.1.2 shows the luminosity for RHIC-II parameters (Table I.A.1.2) based on the present approach of the non-magnetized cooling. For present RHIC operation without electron cooling, β^* (the beta function at the IP) is limited to about one meter (or slightly less), because the emittance is increased by a factor of two due to IBS. Further reduction of β^* with such an increase of the emittance would lead to a significant angular spread and beam loss. On the other hand, keeping the rms emittance constant (by cooling), allows one to begin a store cycle with smaller values of β^*. This is taken into account in Fig. I.A.1.2, where $\beta^*=0.5$ and 1 m were used with and without electron cooling, respectively.

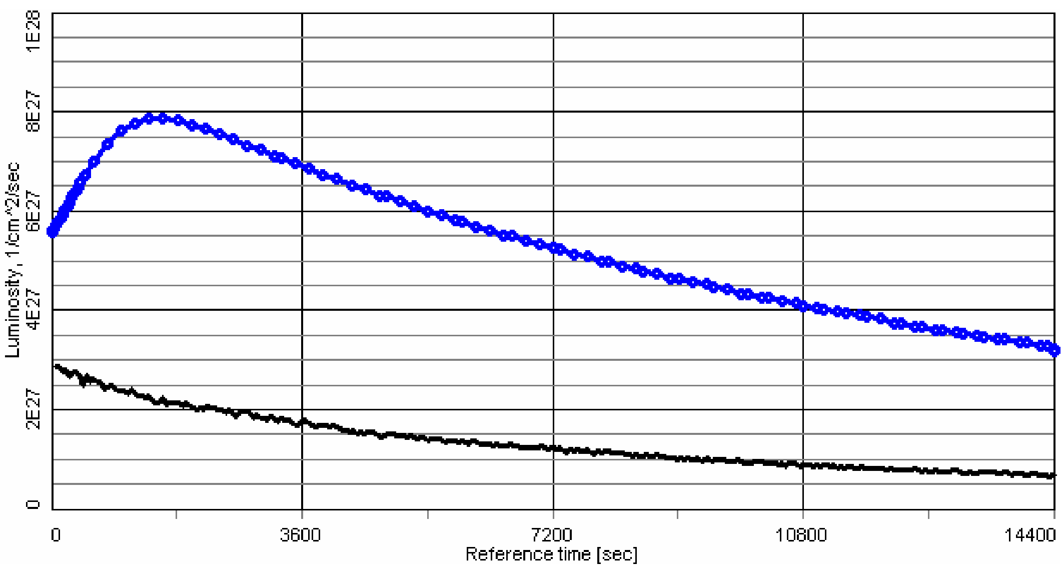

Fig. I.A.1.2: Simulated luminosity for the RHIC-II upgrade, with (blue top curve) and without (black bottom curve) electron cooling, taking $\beta^*=0.5$ m and 1 m, respectively.

The average luminosity with cooling in Fig. 1.A.1.2 (using parameters in Table I.A.1.2) is only $\langle L \rangle = 5.4 \cdot 10^{27}$ [$cm^2 sec^{-1}$], which can be increased by using larger charge of the electron beam and smaller beta-function at the IP, as discussed in Section I.A.5. Also, this number is a low-limit estimate based on a treatment of an rms dynamics. More accurate simulations, based on the details of the distribution, are described in Section I.A.5. Simulations based on detailed dynamics predict larger average luminosity (by 20-30%) but the uncertainty of various algorithms and numerical effects becomes larger as well. All this is summarized in Section I.A.5.

I.A.1.2. Non-magnetized vs magnetized cooling

The traditional electron cooling system employed at any low-energy cooler is based on electron beam generated with an electrostatic electron gun in DC operating mode, immersed in a longitudinal magnetic field. The magnetic field is used for the transport of an electron beam through the cooling section from the gun to the collector. The magnetic field value is determined by condition of electron "magnetization" – radius of the electron Larmor rotation in the transverse plane has to be much less than the beam radius. The presence of a strong longitudinal magnetic field changes the collision kinetics significantly. The magnetic field limits transverse motion of the electrons. In the limit of a very strong magnetic field, the transverse degree of freedom does not take part in the energy exchange, because collisions are adiabatically slow relative to the Larmor oscillations. As a result, the efficiency of electron cooling is determined mainly by the longitudinal velocity spread of the electrons. Such a type of cooling is typically referred to as a "magnetized cooling". Magnetized cooling was found extremely useful technique in obtaining high-brightness hadron beams with extremely low longitudinal momentum spread [5].

However, if an rms velocity spread within electron beam is comparable or smaller than the spread within the ion beam and, and there is no requirement of getting ultra-cold ion state, the cooling can be done without the help of the strong external magnetic field. Such type of cooling is referred to as the "non-magnetized cooling", although weak external field can be still employed, for example, to ensure focusing and alignment of electron and ion beams.

The first cooling system which is based on the "non-magnetized" approach was successfully constructed at FNAL Recycler ring. It is in operation since July 2005. The Recycler's cooling system is also the cooler with the highest energy of the electrons presently in operation (4.3 MeV) [3].

Although extensive studies of the magnetized cooling approach for RHIC showed that such approach is feasible [4, 6] and would provide required luminosities for the RHIC-II, the baseline was recently changed to the non-magnetized one.

Electron cooling at RHIC using the non-magnetized electron beam significantly simplifies the cooler design. Generation and acceleration of the electron bunch without longitudinal magnetic field allows to reach a low value of the emittance for the electron beam in the cooling section. The cooling rate required for suppression of the Intra-Beam Scattering (IBS) can be achieved with a relatively small charge of the electron bunch ~ 5 nC ($3\cdot10^{10}$ electrons per bunch).

For cooling of Au ions in RHIC at the beam energy of 100 GeV/n, the kinetic energy of the electron beam has to be 54.3 MeV. Such a high-energy electron cooling system for RHIC is based on the Energy Recovery Linac (ERL) [7].

I.A.1.3. Parameters of electron cooler

Table I.A.1.2. Ion and electron beam parameters

Ion rms beam emittance normalized [π·mm·mrad]	2.5
Ion rms momentum spread	$5\cdot10^{-4}$
Number of ions per bunch	10^{9}

Ion beta functions in the cooling section [m]	400
Ion rms beam radius [mm]	3
Ion initial rms bunch length [cm]	20
Circumference of RHIC ring [m]	3833
Electron cooler length [m]	80
Electron rms beam emittance normalized [π·mm·mrad]	4
Electron rms momentum spread	$3{\cdot}10^{-4}$
Number of electrons per bunch	$3{\cdot}10^{10}$
Electron rms beam radius [mm]	4.3
Electron rms bunch length [cm]	1
Relativistic factor γ (ions, electrons)	107.35

Table I.A.1.3. Ion and electron beam rms velocities (PRF) corresponding to Table I.A.1.2:

Ion transverse rms velocity [m/s]	$2.5{\cdot}10^{5}$
Ion longitudinal rms velocity [m/s]	$1.5{\cdot}10^{5}$
Electron transverse rms velocity [m/s]	$2.8{\cdot}10^{5}$
Electron longitudinal rms velocity [m/s]	$9.0{\cdot}10^{4}$

I.A.1.4. Suppression of recombination with undulators

Non-magnetized cooling is based on the fact that one can achieve a low temperature of the electrons in the cooling section. However, a general problem of such an approach is high recombination rate for low electron temperature [4].

Presently, suppression of the ion recombination for RHIC is considered using an undulator field in the cooling section [8, 9]. In the presence of an undulator field, trajectories of all electrons have the same coherent azimuth angle θ, determined by the undulator period λ and field value B at the axis:

$$\theta = \frac{eB\lambda}{2\pi pc}, \qquad \text{(I.A.1.1)}$$

where p is the electron momentum.

The recombination coefficient, determined via recombination cross section σ as

$$\alpha_r = \int (V_i - v_e)\sigma(V_i - v_e) f(v_e) d^3 v_e , \qquad \text{(I.A.1.2)}$$

has to be calculated taking into account the coherent transverse electron velocity. Therefore, one can expect sufficient suppression of the recombination without significant loss in the friction force (see Section I.A.2.4).

To provide an estimate of an undulator efficiency we use the BETACOOL program with calculation of the friction force and recombination rates based on numerical evolution of the integrals over the electron velocity distribution. For an accurate estimate of the loss due to recombination one should take into account that the intensity of the ion beam is sharply decreasing due to beam-beam collisions with disintegration in the IP region. Such disintegration (burn-off) depends on the distribution function of the ion beam which one gets as a result of Intra-beam Scattering (IBS) and cooling. All together, these dynamics processes (IBS, cooling, burn-off, recombination) are included in BETACOOL and provide an estimate of the loss due to the recombination.

I.A.2 Friction force description

I.A.2.1. Non-magnetized friction force calculation

In the particle rest frame (PRF) the friction force acting on the ion with a charge number Z passing through an electron beam of density of n_e can be accurately evaluated by numerical integration of the following formula [10, 11]:

$$\vec{F} = -\frac{4\pi n_e e^4 Z^2}{m} \int \ln\left(\frac{\rho_{\max}}{\rho_{\min}}\right) \frac{\vec{V} - \vec{v}_e}{\left|\vec{V} - \vec{v}_e\right|^3} f(v_e) d^3 v_e, \qquad \text{(I.A.2.1)}$$

where e and m are the electron charge and mass, V and v_e are the ion and electron velocities respectively. The Coulomb logarithm $\ln \frac{\rho_{\max}}{\rho_{\min}}$ is kept under the integral because the minimal impact parameter depends on electron velocity:

$$\rho_{\min} = \frac{Ze^2}{m} \frac{1}{\left|\vec{V} - \vec{v}_e\right|^2}. \qquad \text{(I.A.2.2)}$$

At a given value of the ion velocity the maximum impact parameter is constant and determined by either the dynamic shielding radius or the ion time of flight through the electron cloud. Radius of the dynamic shielding sphere coincides with the Debye radius

$$\rho_D = \frac{\Delta_e}{\omega_p}, \qquad \text{(I.A.2.3)}$$

when the ion velocity is less than the electron velocity spread Δ_e. The plasma frequency ω_p is equal to

$$\omega_p = \sqrt{\frac{4\pi n_e e^2}{m}}. \qquad \text{(I.A.2.4)}$$

When the ion velocity is larger than the electron velocity spread, the shielding distance is given by:

$$\rho_{sh} = \frac{V}{\omega_p}. \qquad \text{(I.A.2.5)}$$

The formulae (I.A.2.3) and (I.A.2.5) can be combined together to have a smooth dependence of the shielding radius on the ion velocity:

$$\rho_{sh} = \frac{\sqrt{V^2 + \Delta_e^2}}{\omega_p}. \qquad \text{(I.A.2.6)}$$

In the case when the shielding sphere does not contain large number of electrons to compensate the ion charge (such a situation takes a place, for example, in the case of the magnetized electron beam at low longitudinal velocity spread) it has to be increased in accordance with the electron beam density and the ion charge. In the BETACOOL program such a radius is estimated from the expression

$$n_e \rho^3 \sim 3Z. \qquad \text{(I.A.2.7)}$$

As a result, the maximum impact parameter is calculated as a minimum from three values:

$$\rho_{\max} = \min\left\{ \max\left(\rho_{sh},\ \sqrt[3]{\frac{3Z}{n_e}} \right), V\tau \right\}. \qquad \text{(I.A.2.8)}$$

The second term describes the distance, which the ion passes inside the electron beam. Here τ is the ion time of flight through the cooling section in the PRF:

$$\tau = \frac{l_{cool}}{\beta\gamma c}. \qquad \text{(I.A.2.9)}$$

In the case of an axial symmetry the electron distribution function can be written in the following form:

$$f(v_e) = \left(\frac{1}{2\pi}\right)^{3/2} \frac{1}{\Delta_\perp^2 \Delta_\parallel} \exp\left(-\frac{v_\perp^2}{2\Delta_\perp^2} - \frac{v_\parallel^2}{2\Delta_\parallel^2} \right), \qquad \text{(I.A.2.10)}$$

where $\Delta_\perp$ and $\Delta_\parallel$ are the electron rms velocity spreads in the transverse and longitudinal direction, respectively. The shielding cloud in this case has an ellipsoidal shape which can be approximated by the sphere with the radius, calculated using effective electron velocity spread:

$$\Delta_e^2 = \Delta_\perp^2 + \Delta_\parallel^2. \qquad \text{(I.A.2.11)}$$

The components of the friction force (I.A.2.1) can be evaluated in cylindrical co-ordinate system as follows [1]:

$$F_\perp = -\sqrt{\frac{2}{\pi}} \frac{Z^2 e^4 n_e}{m \Delta_\perp^2 \Delta_\parallel} \int_0^\infty \int_{-\infty}^\infty \int_0^{2\pi} \ln\left(\frac{\rho_{\max}}{\rho_{\min}}\right) \frac{(V_\perp - v_\perp \cos\varphi) \exp\left(-\frac{v_\perp^2}{2\Delta_\perp^2} - \frac{v_\parallel^2}{2\Delta_\parallel^2} \right)}{\left((V_\parallel - v_\parallel)^2 + (V_\perp - v_\perp \cos\varphi)^2 + v_\perp^2 \sin^2\varphi \right)^{3/2}} v_\perp d\varphi dv_\parallel dv_\perp,$$

$$F_\parallel = -\sqrt{\frac{2}{\pi}} \frac{Z^2 e^4 n_e}{m \Delta_\perp^2 \Delta_\parallel} \int_0^\infty \int_{-\infty}^\infty \int_0^{2\pi} \ln\left(\frac{\rho_{\max}}{\rho_{\min}}\right) \frac{(V_\parallel - v_\parallel) \exp\left(-\frac{v_\perp^2}{2\Delta_\perp^2} - \frac{v_\parallel^2}{2\Delta_\parallel^2} \right)}{\left((V_\parallel - v_\parallel)^2 + (V_\perp - v_\perp \cos\varphi)^2 + v_\perp^2 \sin^2\varphi \right)^{3/2}} v_\perp d\varphi dv_\parallel dv_\perp. \qquad \text{(I.A.2.12)}$$

Within an accuracy of about 2% the upper limit of the integrals over velocity components can be replaced from infinity to three corresponding rms values, and an integration over φ can be performed from 0 to π due to symmetry of the formulae. In this case the friction force components can be calculated as (such expressions are used in BETACOOL):

$$F_{\perp} = -\frac{4\pi Z^2 e^4 n_e}{m \cdot Int} \int_0^{3\Delta_\perp} \int_{-3\Delta_\parallel}^{3\Delta_\parallel} \int_0^{\pi} \ln\left(\frac{\rho_{\max}}{\rho_{\min}}\right) \frac{(V_\perp - v_\perp \cos\varphi)\exp\left(-\frac{v_\perp^2}{2\Delta_\perp^2} - \frac{v_\parallel^2}{2\Delta_\parallel^2}\right)}{\left((V_\parallel - v_\parallel)^2 + (V_\perp - v_\perp \cos\varphi)^2 + v_\perp^2 \sin^2\varphi\right)^{3/2}} v_\perp d\varphi dv_\parallel dv_\perp ,$$

$$F_{\parallel} = -\frac{4\pi Z^2 e^4 n_e}{m \cdot Int} \int_0^{3\Delta_\perp} \int_{-3\Delta_\parallel}^{3\Delta_\parallel} \int_0^{\pi} \ln\left(\frac{\rho_{\max}}{\rho_{\min}}\right) \frac{(V_\parallel - v_\parallel)\exp\left(-\frac{v_\perp^2}{2\Delta_\perp^2} - \frac{v_\parallel^2}{2\Delta_\parallel^2}\right)}{\left((V_\parallel - v_\parallel)^2 + (V_\perp - v_\perp \cos\varphi)^2 + v_\perp^2 \sin^2\varphi\right)^{3/2}} v_\perp d\varphi dv_\parallel dv_\perp , \quad \text{(I.A.2.13)}$$

where the normalization factor is calculated in accordance with:

$$Int = \int_0^{3\Delta_\perp} \int_{-3\Delta_\parallel}^{3\Delta_\parallel} \int_0^{\pi} \exp\left(-\frac{v_\perp^2}{2\Delta_\perp^2} - \frac{v_\parallel^2}{2\Delta_\parallel^2}\right) v_\perp d\varphi dv_\parallel dv_\perp . \quad \text{(I.A.2.14)}$$

The minimal impact parameter is the following function of the electron velocity components:

$$\rho_{\min} = \frac{Ze^2}{m_e} \frac{1}{(V_\parallel - v_\parallel)^2 + (V_\perp - v_\perp \cos\varphi)^2 + v_\perp^2 \sin^2\varphi} . \quad \text{(I.A.2.15)}$$

When the Coulomb logarithm L_C is constant the two of the three integrals in Eq. (I.A.2.12) can be calculated analytically and the friction force components can be written in accordance with Binney's formulae [12]. Such an algorithm significantly speeds up numerical evaluation of the friction force and is also included in the BETACOOL code.

I.A.2.2. Comparison with direct numeric simulation

The first step towards accurate calculation of cooling times is to use an accurate description of the cooling force. As for the previous case of the magnetized cooling, the VORPAL code [2] is being used to simulate from first principles the non-magnetized friction force and diffusion coefficients for the parameters of the RHIC cooler. For simulation of electron cooling problem, VORPAL uses molecular dynamics techniques and explicitly resolves close binary collisions to obtain the friction force and diffusion coefficient with a minimum of physical assumptions [13].

The latest version of the BETACOOL code [1] includes direct numerical integration over the electron velocity distribution. This numerical evaluation of the force enables an accurate comparison with the VORPAL results, both for the magnetized and non-magnetized friction force with an anisotropic velocity distribution of the electrons. The results of such benchmarking are summarized in [14, 15].

For example, Fig. I.A.2.1 compares VORPAL data (dots with error bars) with the result of numerical integration based on Eq. (I.A.2.1) (solid red line), for the case of an anisotropic Maxwellian velocity distribution of the electrons given in Eq. (I.A.2.10), where $\Delta_{\perp}=4.2\cdot10^{5}$ [m/s] and $\Delta_{\|}=1.0\cdot10^{5}$ [m/s] ($Z=79$, $n_e=2\cdot10^{15}$ m^{-3}).

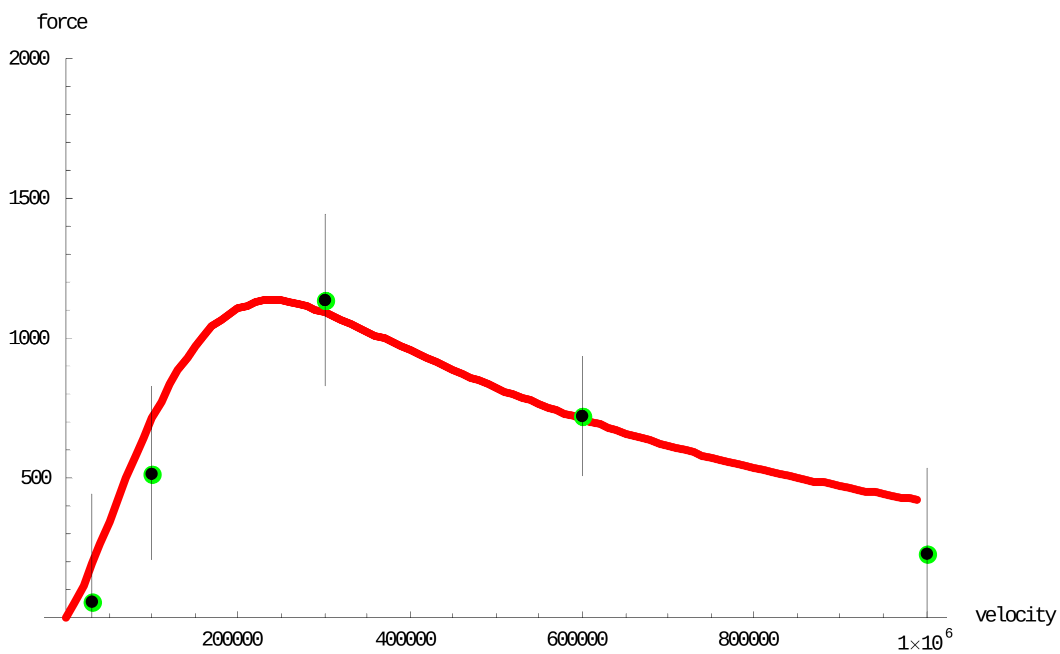

Fig. I.A.2.1. Non-magnetized friction force for an anisotropic electron velocity distribution. Force [eV/m] vs. ion velocity [m/s]: solid line (red) – numeric integration using BETACOOL; points with errors bar (3 rms deviation shown)– simulations using VORPAL.

Simulations were done for other degrees of anisotropy of the electron velocity as well. We find agreement between VORPAL simulations and numeric integration satisfactory, and thus use the non-magnetized friction force in BETACOOL (based on numerical evaluation of the integrals) in our simulations of the non-magnetized cooling.

I.A.2.3. Comparison with experimental data

In a typical low-energy electron cooling system a longitudinal magnetic field is used for transportation of the electron beam. For decreased values of the magnetic field in the cooling section the beam quality is diminished and investigation of the non-magnetized regime of the electron cooling can not be provided with a well controlled conditions.

In July 2005 the Recycler cooling system was put into operation in Fermilab [3]. In Recycler's cooling system the longitudinal magnetic field in the cooling section is used only to preserve angular spread of the electrons θ at the level below 200 μrad. The required longitudinal magnetic field value B is about 105 G that corresponds to electron rotation with Larmor radius

$$\rho_{\perp} = \frac{pc}{eB}\theta \approx 3\cdot10^{-4}\, m\,,$$

where pc = 4.85 MeV is the electron momentum. The cooling section length is 20 m which approximately corresponds to 2 steps of the Larmor helix. A maximum impact parameter for the maximum electron current of 500 mA is restricted by a time of flight through the cooling section and it is equal

$$\rho_{\max} \approx 7 \cdot 10^{-5} m,$$

which is smaller than the electron Larmor radius. At such parameters one can expect that an impact of the magnetized collisions on the friction force is negligible.

To provide an accurate comparison between the results of the experimental studies at Recycler (FNAL) and numerical simulation within the BETACOOL, several new algorithms were implemented in the code. A general method for the friction force measurements at the Recycler is Voltage Step method. Such a procedure was also explored within the BETACOOL.

One of the features of the Recycler cooling system is strong dependence of the electron transverse velocity spread on the distance from the beam centre. This effect appears due to the beam envelope mismatch with the transport channel, and is called "envelope scalloping". In the first approximation this effect can be presented as a linear increase of the velocity spread with radial co-ordinate:

$$\Delta_{\perp} = \frac{d\Delta_{\perp}}{dr} r, \qquad \text{(I.A.2.16)}$$

where the velocity gradient $\frac{d\Delta_{\perp}}{dr}$ is an additional input parameter available in BETACOOL simulations.

An example of simulations of the cooling (using BETACOOL) is presented in the Fig. I.A.2.2. The red curve correspond to an average momentum of the antiprotons. The first 1700 sec correspond to pre-cooling of the antiprotons. At t=1700 sec, the electron momentum was shifted by the relative value of 10^{-3} and during the next 2000 sec the average antiproton momentum is cooled to the new momentum of the electrons. The green curve presents the variation in time of the antiproton momentum spread.

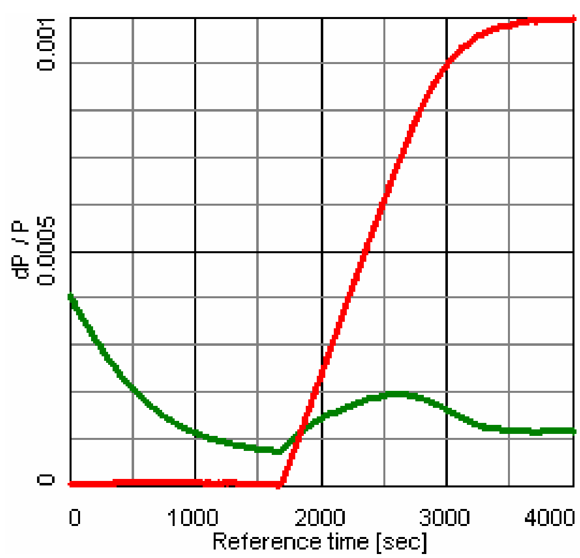

Fig. I.A.2.2. Simulation of the voltage step method using BETACOOL program, for the parameters shown in Table I.A.2.1.

Table I.A.2.1. The cooling system parameters used in simulations.

Cooling section length, m	20
Electron energy, MeV	4.36
Beta functions in the cooling section, m	20
Electron current, A	0.2
Electron beam radius, cm	0.45
Transverse temperature (PRF), eV	0.5
Longitudinal temperature (PRF), eV	0.01

Evolution of the antiproton momentum during the friction force measurement, as a 3D plot of the profile versus time, is shown in Fig I.A.2.3.

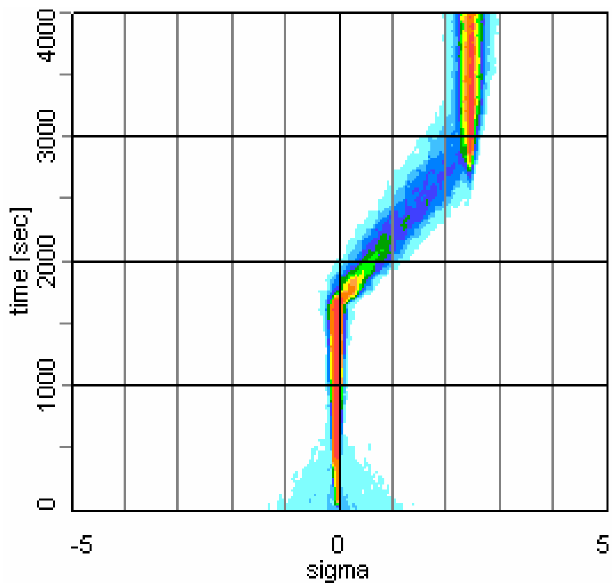

Fig. I.A.2.3. The longitudinal profile evolution during friction force measurement.

To reproduce the procedure used in Fermilab for the beam longitudinal distribution measurement the possibility to average over a few consequent longitudinal profiles was also introduced. An example of a few consequent averaged profiles calculated with BETACOOL after 2 keV step of the electron energy is presented in the Fig. I.A.2.4. The electron beam current is 500 mA. Figure I.A.2.5 shows measured profiles for the same parameters.

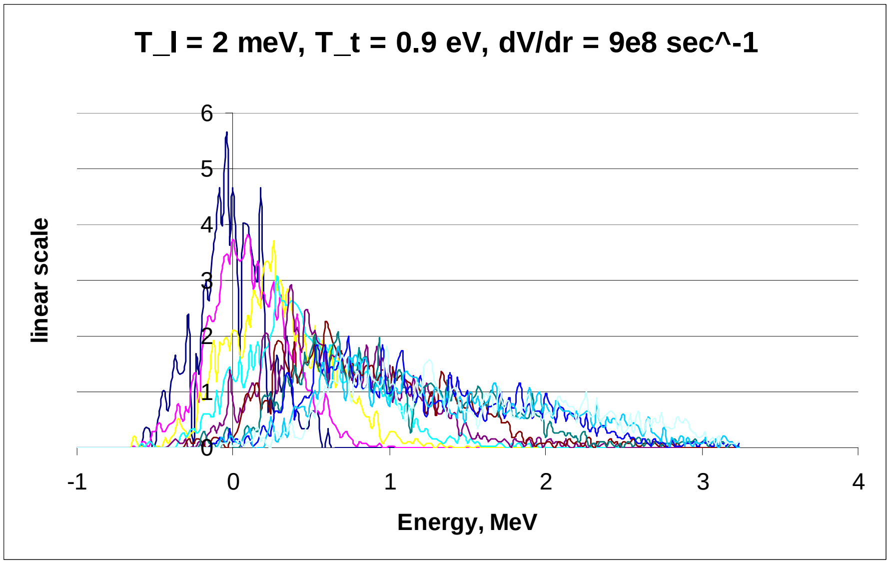

Fig. I.A.2.4. Simulations (A. Sidorin). Evolution of the longitudinal profile in time. Distance between slices is 50 sec.

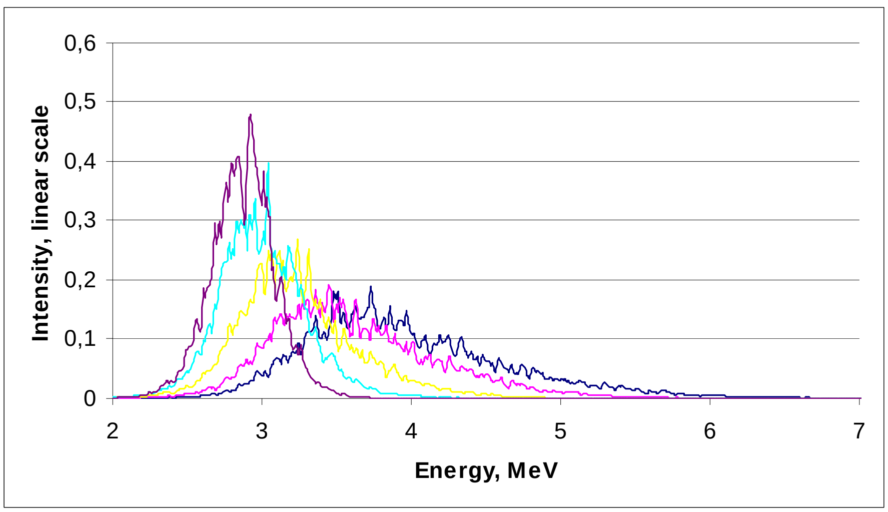

Fig. I.A.2.5. Measurements (L. Prost, 10/31/05). Evolution of the longitudinal profile in time.

Analysis of the experimental data and comparison with theory was done in collaboration with the Electron cooling group of Fermilab (S. Nagaitsev, L. Prost, A. Shemyakin, A. Burov). In general, we find agreement between the theory and experiments to be very good – within 20-30%, depending on assumptions for the electron beam parameters being used. More details on the results of benchmarking can be obtained from the Fermilab group [16].

I.A.2.4. Friction force in the presence of an undulator field

Suppression of the ion recombination for RHIC is based on the use of an undulator field in the cooling section [8, 9]. In the presence of an undulator field, the trajectories of all the electrons have the same coherent azimuthal angle θ, determined by the undulator period λ and field value B at the axis:

$$\theta = \frac{eB\lambda}{2\pi pc}, \qquad \text{(I.A.2.17)}$$

where p is the electron momentum. Since the recombination cross section is approximately inversely proportional to the electron energy in the ion rest frame, the ion beam life time can be sufficiently improved.

One can expect that at impact parameters significantly larger than the electron rotation radius

$$r_0 = \frac{\theta\lambda}{2\pi} = \frac{eB\lambda^2}{4\pi^2 pc} \qquad \text{(I.A.2.18)}$$

kinematics of the binary collisions will be similar to Rutherford scattering of free electron. In this case the friction force acting on the ion inside the electron beam with the velocity distribution function $f(v_e)$ can be still calculated with the usual formula:

$$\vec{F} = -\frac{4\pi n_e e^4 Z^2}{m} \int L \frac{\vec{V}_i - \vec{v}_e}{\left|\vec{V}_i - \vec{v}_e\right|^3} f(v_e) d^3 v_e, \qquad \text{(I.A.2.19)}$$

where n_e is electron density in the Particle Rest Frame (PRF), v_e, V_i are the electron and ion velocity, L – Coulomb logarithm:

$$L = \ln \frac{\rho_{\max}}{\rho_{\min}}. \qquad \text{(I.A.2.20)}$$

For the RHIC parameters, the maximum impact parameter is determined by the time of flight of the ion through the cooling section and it is not affected by the undulator field. However, the minimum impact parameter ρ_{min} which is determined by a relative velocity between an ion and electron as

$$\rho_{\min} = \frac{Ze^2}{m_e} \frac{1}{\left|\vec{V}_i - \vec{v}_e\right|^2}, \qquad \text{(I.A.2.21)}$$

has to be replaced by r_0 value, in the presence of the undulator field. Therefore, the friction force is expected to be reduced by the factor of the order of $\ln \frac{\rho_{\max}}{\rho_{\min}} / \ln \frac{\rho_{\max}}{r_0}$.

To make sure that such a representation of the friction force in the presence of an undulator field is accurate, an undulator field was implemented in the VORPAL code, and numerical simulations were performed (G. Bell et al.) [17] for different strength of the magnetic field B and pitch period λ. In all cases, it was found that the friction force scales as predicted by a modified logarithm $\ln \frac{\rho_{\max}}{r_0}$.

An example of such a comparison between VORPAL simulations (dots with error bars) and numeric integration with the BETACOOL (lines) is shown in Figs. I.A.2.6-7, for an rms ion velocity of $3.0 \cdot 10^5$ [m/s] in PRF and the following parameters in simulations ($\Delta_\perp = 3.0 \cdot 10^5$ [m/s] and $\Delta_\parallel = 3.0 \cdot 10^5$ [m/s], $\tau = 0.9$ nsec, Z=79, $n_e = 7.32 \cdot 10^{13}$ m^{-3}).

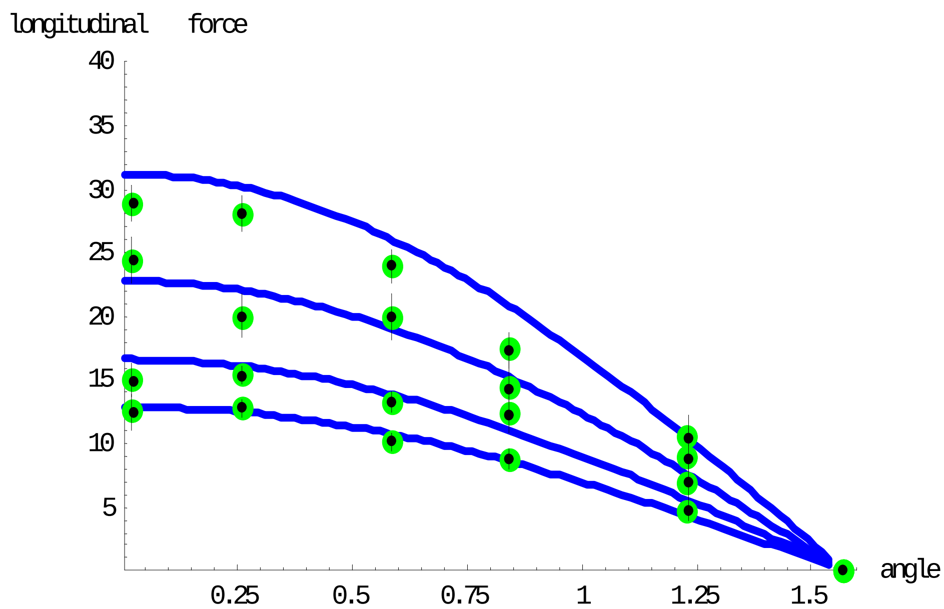

Fig. I.A.2.6. Longitudinal component of the friction force at an rms ion velocity of $3.0 \cdot 10^5$ m/s for B=0 (upper curve) and for an undulator with different periods λ=8, 16, 24 cm (B=10G). VORPAL – dots with error bars; BETACOOL numerical integration –lines.

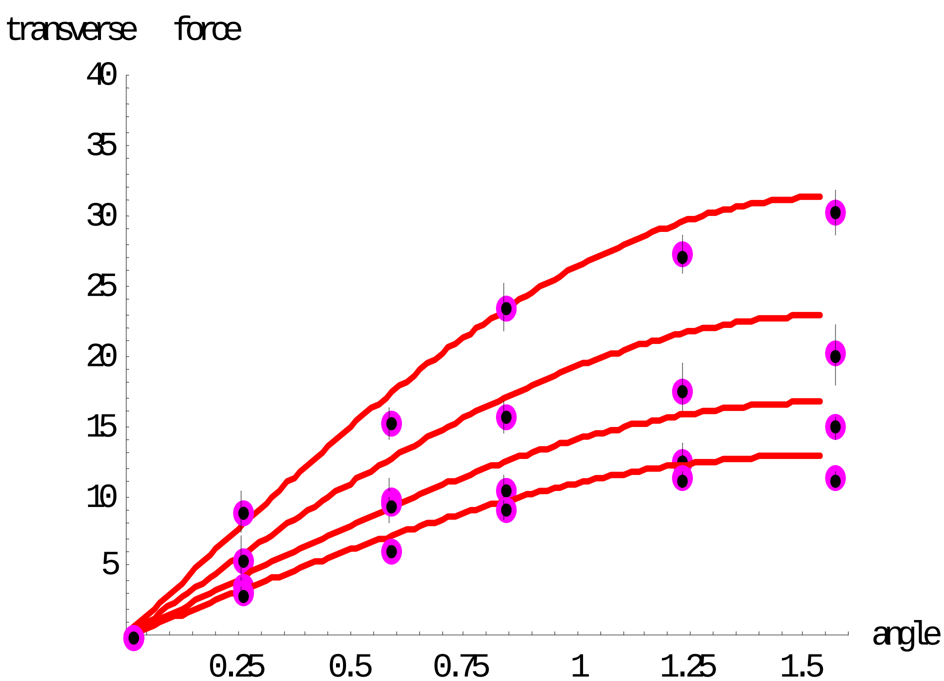

Fig. I.A.2.7. Transverse component of the friction force at an rms ion velocity of $3.0 \cdot 10^5$ m/s for B=0 (upper curve) and for an undulator with different periods λ=8, 16, 24 cm (B=10G). VORPAL – dots with error bars; BETACOOL numerical integration – lines.

I.A.3. Intrabeam scattering

Charged particle beam are stored in circular accelerators for a long time. The phenomenon when particles within the beam are scattered from one another via Coulomb scattering is called Intra-Beam Scattering (IBS). Such a process is typically separated in two effects:

1. Scattering on a large angle so that the particles can be lost from a bunch as a result of a single collision – such an effect is called the Touschek effect.

2. Scattering on small angles can randomly add together which can cause beam dimension to grow – such effect is called the Intra-Beam Scattering.

I.A.3.1 General models

The process of IBS is very similar to collisions in a plasma (ionized gas), which govern gas relaxation towards equilibrium. The corresponding simple diffusion coefficients can be derived. The case of charged particle beam is in fact very similar to the plasma case when the longitudinal motion is transformed away by going into the Particle-Rest-Frame (PRF) which moves along the storage ring at the nominal beam velocity. The scattering events now appear exactly as in the plasma case, the only difference is that the distribution function is now given in terms of generalized coordinates which describe particle motions in circular accelerator . In circular accelerator, curvature of the orbit produces a dispersion, and due to the dispersion a sudden change in energy results in a change of betatron amplitudes. Such a coupling makes an important difference between small-angle Coulomb collisions in plasma (Gas-Relaxation) and in circular accelerators (IBS).

A theory of IBS for protons beams was proposed by Piwinski [18], who calculated the beam growth rates in all three dimensions. In the original theory, growth rates were estimated as an average around the circumference of the ring. For this purpose, the ring lattice functions were also averaged. This model was later extended by a CERN team in collaboration with Piwinski to include variations of the lattice function around the ring. An improved model was later described in a detailed report by Martini [19] and is sometimes referred to as Martini's model. Similar results were also obtained with a completely different approach of S-matrix formalism by Bjorken and Mtingwa [20].

For RHIC parameters, results using both Martini's and Bjorken-Mtingwa's models were found to be in a very good agreement with one another. For our numerical studies of electron cooling presented in this report the Martini's model was used without any approximation. We also used an exact designed lattice of RHIC which includes the derivatives of the lattice functions and insertions in the straight sections for the IP's.

The standard IBS theories were developed in the assumption of uncoupled betatron motion. A more general treatment for the coupled motion was also developed by Piwinski [18] and recently by Lebedev [21]. The standard RHIC operation corresponds to the working point in the vicinity of the coupling resonance with the fully coupled motion. In such a case, the standard treatment of IBS can be used with the horizontal growth rate equally shared between the horizontal and vertical motion – such an assumption was found to be in good agreement with experimental measurements and is presently used in simulations.

I.A.3.2 IBS in RHIC: experiments vs theory

Since the main goal of electron cooling is to overcome emittance growth due to IBS, it was extremely important to make sure that the models of IBS which are being used in cooling simulations are in a good agreement with experimentally measured growth rates.

Several dedicated IBS experiments were performed in 2004 with Au and in 2005 with Cu ions with an intention to increase accuracy and parameter range of previous measurements [22]. To ensure an accurate benchmarking of the IBS models, bunches of various intensity and emittance were injected, and growth rates of both the horizontal and vertical emittance and the bunch length were recorded with IPM and WCM, respectively. Other effects which may obscure comparison, like beam-beam collisions, were switched off. Experiments were done with the RF harmonic h=360 allowing growth of the longitudinal profile without any loss from the bucket.

Although, agreement for the longitudinal growth rate was very good for the 2004 measurements with the Au ions, agreement for the transverse emittance was not that perfect [23]. In fact, the measured transverse emittance growth was larger than the one predicted by simulation using Martini’s model of IBS with the exact designed RHIC lattice. As a result of the 2004 studies, a fudge factor was introduced for the transverse growth rate of IBS to make sure that we do not underestimate IBS growth rate for the cooling simulations. Subsequent cooling simulations were done to compensate for such an “enhanced” IBS.

Following the 2004 measurements several studies were done trying to understand a possible source of the disagreement, including IBS growth for the lattice with different average dispersion functions, FODO approximation for the lattice vs. realistic RHIC lattice with straight-section insertions, dispersion mismatch and others [24]. As a result of these studies, it was decided to repeat the measurements with the Cu ions in 2005.

The latest data for IBS with Cu ions showed very good agreement between the measurements and Martini’s model of IBS for designed RHIC lattice without any approximation or previously used fudge factors [25]. Below, few examples from these studies are shown in Figs. I.A.3.1-3.

Figure I.A.3.1 shows growth of the horizontal and vertical emittance in bucket # 100 with the bunch intensity $2.9 \cdot 10^9$.

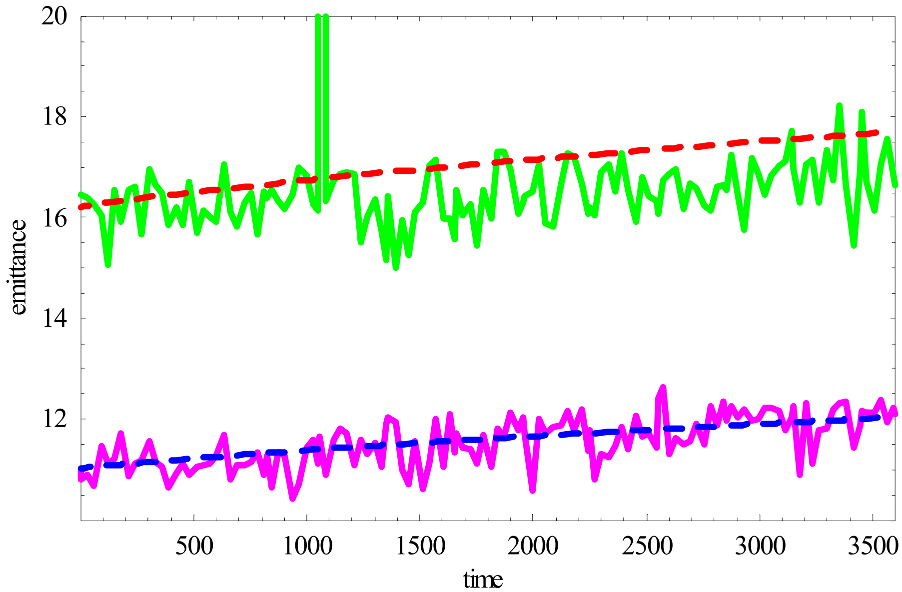

Fig. I.A.3.1 Horizontal (upper curve) and vertical 95% normalized emittance [mm mrad] vs time [sec] for bunch intensity $2.9\cdot10^9$ Cu ions. Measured emittance: green (horizontal), pink (vertical). BETACOOL simulation using Martini's model: red dash line (horizontal), blue dash line (vertical).

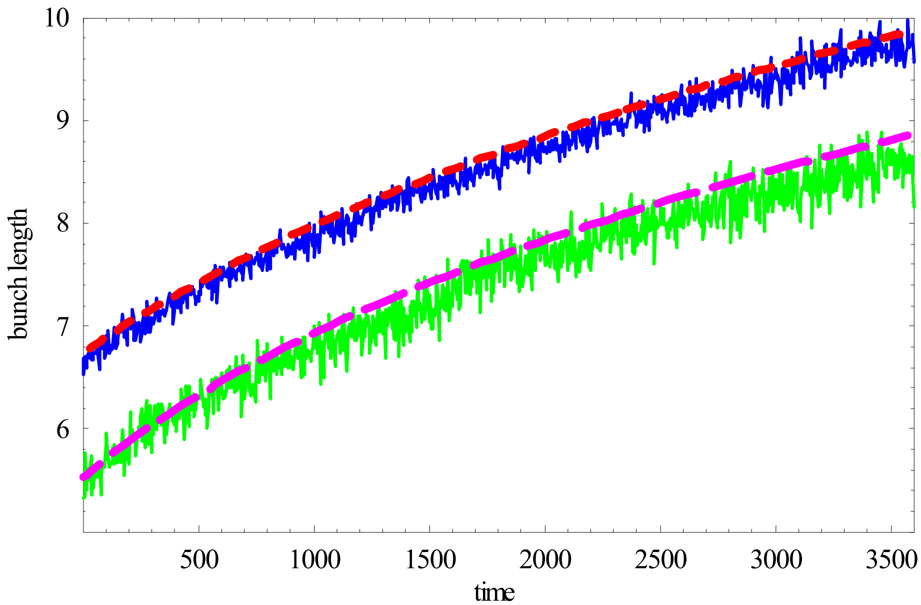

Fig. I.A.3.2 Growth of FWHM bunch length [ns] vs time [sec] for two bunch intensities: $2.9\cdot10^9$ (upper curve) and $1.4\cdot10^9$ (lower curve) Cu ions.

Measured growth rates scale correctly with the bunch intensity and the value of the initial emittance, as shown for the two intensities in Fig. I.A.3.2 and Fig. I.A.3.3 for the bunch length and horizontal emittance, respectively.

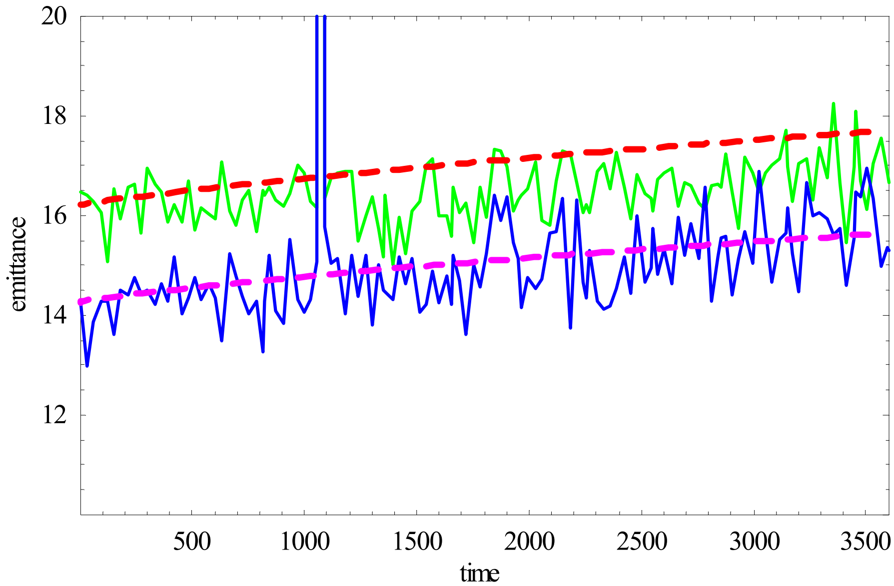

Fig. I.A.3.3 Horizontal 95% normalized emittance [μm] for two bunch intensities: $2.9 \cdot 10^9$ (upper curve) and $1.4 \cdot 10^9$ (lower curve) Cu ions.

More details about comparison of IBS measurements in RHIC with the models can be found in [25].

I.A.3.3 IBS for ion beam distribution under electron cooling

Standard models of IBS discussed above are based on the growth rates of the rms beam parameters for the Gaussian distribution. However, as a result of electron cooling, the core of beam distribution is cooled much faster than the tails. For previous parameters of the magnetized cooling it was found that a simple use of standard rms-based IBS approach would significantly underestimate IBS for beam core. A detailed analytic treatment of IBS, which depends on individual particle amplitude was proposed by Burov [26], with an analytic formulation done for a "flattened" Gaussian distribution. Also, a simplified "core-tail" model, based on a different diffusion coefficients for beam core and tails was also proposed [27]. In addition, the standard IBS theory was reformulated for the rms growth rates of a bi-Gaussian distribution by Parzen [28].

The above formulations, which attempt to calculate IBS for a beam distribution changing under electron cooling, were implemented in BETACOOL [1] and were used for cooling studies of RHIC [27]. The difference between various models and resulting integrated luminosity was found substantial for the previous approach of the magnetized cooling where a formation of a distribution with a sharp core was observed.

For the present parameters of the non-magnetized cooling, the formation of such a bi-Gaussian distribution is less pronounced than before for the case of the magnetized cooling. As a result, a deviation between various models and the difference in the integrated luminosity being predicted is expected to be less crucial, although it is probably the largest source of uncertainty in present simulations. More detailed algorithms for the IBS are presently being developed to reduce remaining uncertainty.

I.A.4 Recombination

I.A.4.1 Numerical algorithm

Ion beam life time due to recombination

The ion beam life time due to recombination in the cooling section is calculated via recombination coefficient α_r by the following formula:

$$\frac{1}{N}\frac{dN}{dt} = -\frac{\alpha_r n_e}{\gamma^2}\frac{l_{cool}}{C}, \qquad \text{(I.A.4.1)}$$

here C is the ring circumference. Under assumption that ion velocity in PRF is substantially less than electron one α_r is calculated in PRF by averaging of the recombination cross section over electron distribution function:

$$\alpha_r = \langle v\sigma(v)\rangle \qquad \text{(I.A.4.2.)}$$

The recombination cross section can be calculated with good accuracy using the following formula:

$$\sigma = A\left(\frac{h\nu_0}{E}\right)\left(\ln\sqrt{\frac{h\nu_0}{E}} + 0.1402 + 0.525\left(\frac{E}{h\nu_0}\right)^{1/3}\right), \qquad \text{(I.A.4.3)}$$

where $A = 2^4 3^{-3/2} he^2/\left(m_e^3 c^2\right)$ = 2.11×10^{-22} cm^2, $h\nu_0 = 13.6\cdot Z^2$ eV is the ion ground state binding energy, and $E = \dfrac{m_e v_e^2}{2}$ is the kinetic energy of the electrons. In the presence of the undulator field the kinetic energy needs to be calculated as:

$$E = \frac{m}{2}\left((v_\perp + v_{und})^2 + v_\parallel^2\right), \qquad \text{(I.A.4.4)}$$

The formula (I.A.4.2) can be rewritten in the form adopted for numerical integration:

$$\alpha_r = \frac{1}{Int}\int_0^{3\Delta_\perp}\int_{-3\Delta_\parallel}^{3\Delta_\parallel}\sigma(E)\sqrt{(v_\perp + v_{und})^2 + v_\parallel^2}\exp\left(-\frac{(v_\perp + v_{und})^2}{2\Delta_\perp^2} - \frac{v_\parallel^2}{2\Delta_\parallel^2}\right)v_\perp dv_\parallel dv_\perp . \text{(I.A.4.5)}$$

The normalization factor is calculated as:

$$Int = \int_0^{3\Delta_\perp}\int_{-3\Delta_\parallel}^{3\Delta_\parallel}\exp\left(-\frac{(v_\perp + v_{und})^2}{2\Delta_\perp^2} - \frac{v_\parallel^2}{2\Delta_\parallel^2}\right)v_\perp dv_\parallel dv_\perp . \qquad \text{(I.A.4.6)}$$

Here

$$\Delta_e = \sqrt{\Delta_\perp^2 + \Delta_\parallel^2} \qquad \text{(I.A.4.7)}$$

is an rms electron velocity spread, with the electron beam temperature being different for the transverse and longitudinal degrees of freedom. The expression in Eq. (I.A.4.5) is being used in BETACOOL to calculate recombination rate for RHIC.

I.A.4.2 Parameters of the undulator

Table I.A.4.1 Parameters of the undulator

Magnetic field [G]	10
Period [cm]	8
Introduced effective temperature Teff [eV]	30
Recombination lifetime with Teff [hours]	166

I.A.5 Detailed calculation of the cooling dynamics

I.A.5.1 Baseline parameters

Table I.A.5.1 Present parameters

Electron kinetic energy [MeV]	54.34
Number of electrons per bunch	$3 \cdot 10^{10}$
Electron charge per bunch [nC]	5
Ion beta functions in the cooling section [m]	400
Ion rms beam radius [mm]	3
Ion initial rms bunch length [cm]	20
Circumference of RHIC ring [m]	3833
Electron cooler length [m]	80
Rms electron beam emittance normalized [π·mm·mrad]	4
Electron rms momentum spread	$3 \cdot 10^{-4}$
Ion initial rms momentum spread	$5 \cdot 10^{-4}$
Transverse rms radius of electron beam [mm]	4.3
Electron rms bunch length [cm]	1
Relativistic factor γ (ions, electrons)	107.35

I.A.5.2 Detailed evolution of beam distribution

A quick estimate of the cooler performance can be done using an approach with a dynamical tracking of the rms beam parameters. This approach was found to be too inaccurate for previous design with the magnetized cooling for RHIC when a detailed treatment of the beam distribution was found to be extremely important. For the case of a fast cooling in typical low-energy coolers where the whole Gaussian beam is quickly cooled to an approximately Gaussian beam with much smaller rms parameters, a simple approach based on an rms dynamics provides reasonably accurate estimates. For the present parameters of the RHIC cooler based on the non-magnetized approach most of the particles within few sigmas are also effectively cooled, making an rms dynamics approach a reasonable estimate as well. The luminosity prediction based on such an rms approach is shown in Fig. I.A.5.1.

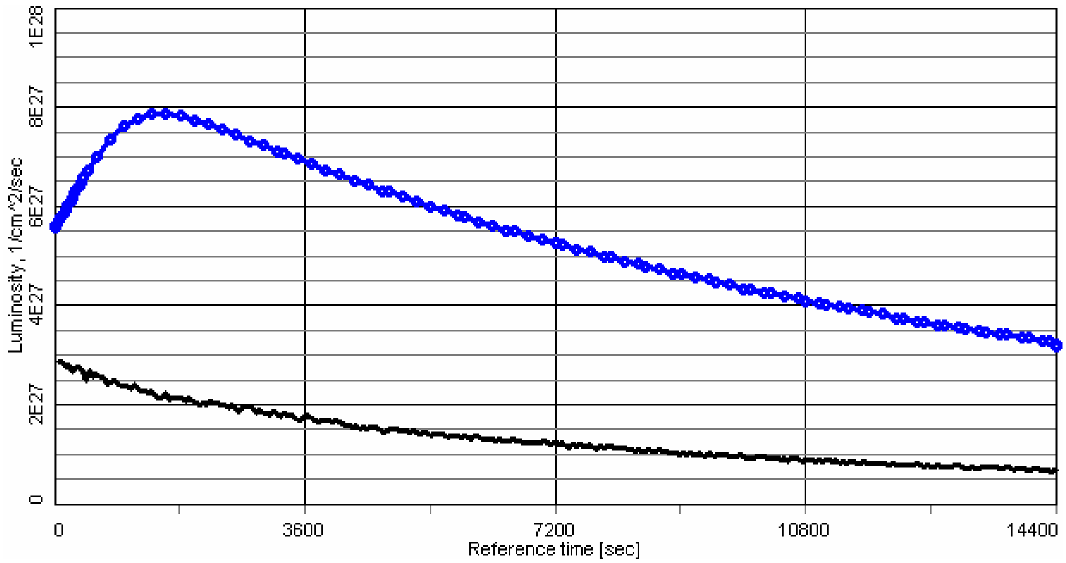

Fig. I.A.5.1 Luminosity for RHIC-II without cooling (black) and with cooling (blue) based on simulations with the rms dynamics, for cooler parameters in Table I.A.5.1.

The average luminosity with cooling in Fig. 1.A.5.1 is only $<L>=5.4\cdot10^{27}$ [cm^2sec^{-1}], which can be increased by using higher charge of the electron beam and smaller beta-function at the IP. For example, by cooling with 10nC electrons one gets $<L>=8\cdot10^{27}$ [cm^2sec^{-1}] per store, and decreasing in addition β^* to 30cm gives $<L>=11\cdot10^{27}$ per store. However, the length of the optimum store now becomes very short (only 2 hours) with the net gain in the average luminosity being less pronounced, which is about factor of 6.5 compared to the luminosity without cooling. Note, that such an estimate is based on the rms dynamics and is a low-limit estimate for the luminosity increase.

A more accurate treatment is to use a numerical approach which allows one to track evolution of the beam distribution. Such an approach requires accurate calculation of many effects from a real distribution, including loss on recombination, burn-off process, IBS and calculation of the luminosity from the local charge density. All these algorithms are implemented in BETACOOL and are being used under the "Modeled beam" approach.

However, each of these effects contributes to the uncertainty (numerical effects and accuracy of the models being used) in the simulations. As a result, an accuracy of predicted average luminosity is probably not better than 10-20%. The effect which results in the largest uncertainty (due to an approximate model) is the treatment of IBS for non-Gaussian distribution. Presently, depending on the model being used, the final result can be different by as much as 20-30%. To remove this largest source of uncertainty new numerical algorithms are being developed within the BETACOOL to describe IBS for an arbitrary distribution more accurately.

Figures I.A.5.2-4 show evolution of the horizontal (red), vertical (blue) and longitudinal (green) beam profiles after 0.5, 1.5 and 2.5 hours of cooling, respectively. Simulations were done for the parameters in Table I.A.5.1 using the "Modeled beam" approach in BETACOOL. The corresponding luminosity with and without cooling is shown in Fig. I.A.5.5.

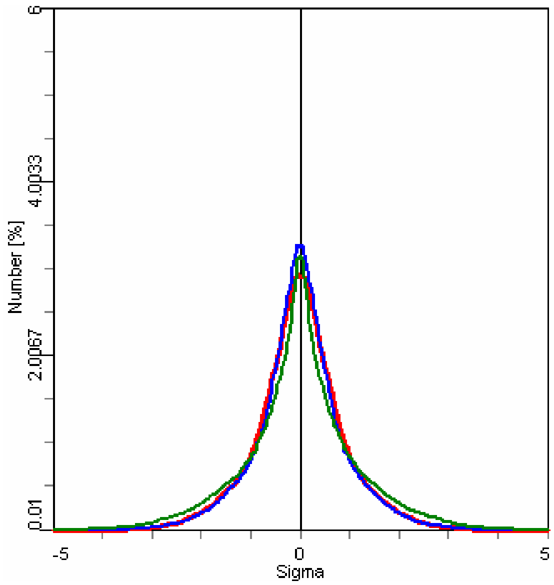

Fig. I.A.5.2 Beam profiles (x-red, y-blue, longitudinal -green) after 30 minutes of cooling

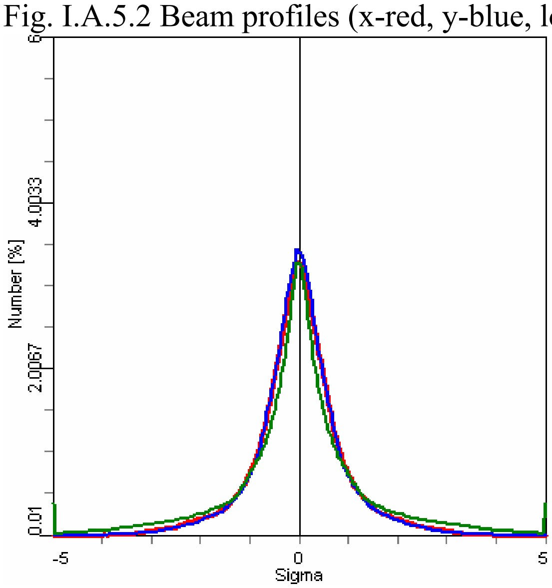

Fig. I.A.5.3 Beam profiles after 1.5 hours of cooling.

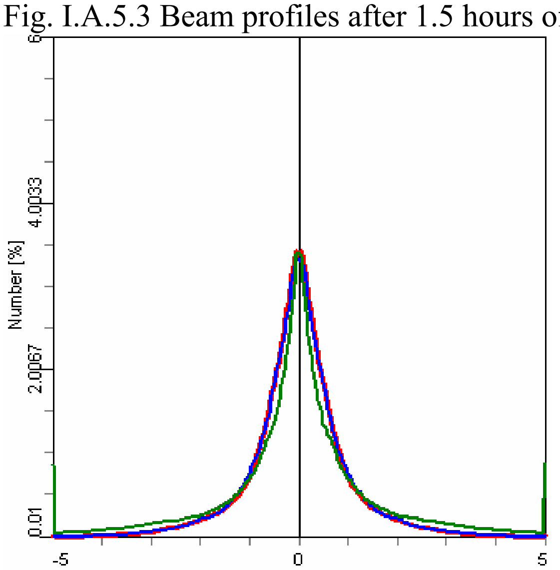

Fig. I.A.5.4 Beam profiles after 2.5 hours of cooling.

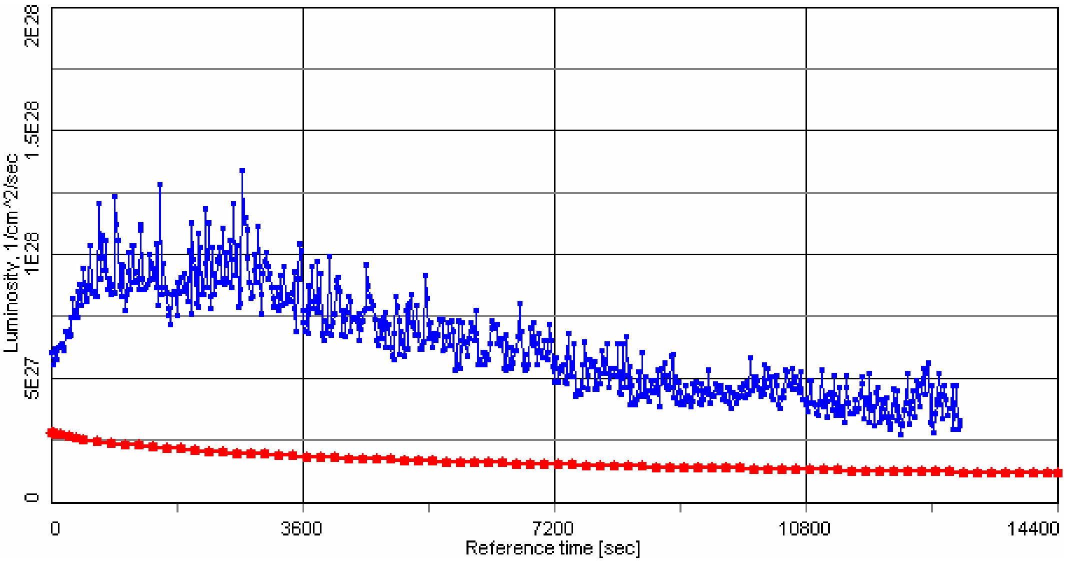

Fig. I.A.5.5 Luminosity with (blue) and without (red) cooling using "Modeled beam" approach in BETACOOL simulations for parameters in Table I.A.5.1.

Although predicted integrated luminosity in Fig. I.A.5.5 appears to be higher than the one predicted based on the rms approach, the uncertainty in its value is larger as well. For the case shown in Fig. I.A.5.5, average luminosity with cooling (blue) per store is $\langle L \rangle = 6.4 \cdot 10^{27}$[cm^{2}sec^{-1}], which is 20% higher than based on the rms dynamics estimate.

An additional luminosity increase comes from the painting with the electron beam (which we need to do since the length of the electron bunch is much smaller than the one of the ions), which is discussed in Section I.A.6. For parameters used in Fig. I.A.5.5 but with painting one gets $\langle L \rangle = 7.3 \cdot 10^{27}$[cm^{2}sec^{-1}].

I.A.5.3 Requirements on transverse emittance of electron beam

Ideally, one would like to have the transverse rms velocity spread of the electron beam to be comparable or smaller than the one of the ions. Since the normalized rms emittance of ions is 2.5 μm an ideal electron emittance should be slightly below 2.5 μm. However, the necessary cooling power requires charge within electron bunch to be around 5nC. A preliminary simulations with electron beam showed that the electron emittance of 4 μm can be achieved. The sizes of the ion and electron beam in the cooling section were optimized so that the rms normalized emittance of 4 μm provides sufficient cooling power.

I.A.5.4 Requirements on longitudinal momentum spread of electron beam

The rms momentum spread of the ion beam is about $0.5 \cdot 10^{-3}$. An effective longitudinal cooling is obtained with the rms momentum spread of the electron beam around $0.3 \cdot 10^{-3}$. Simulations were performed to find out requirement on the average electron beam energy. The cooling efficiency was significantly affected when the average energy of the electron beam became comparable or bigger than the rms energy spread of the ion beam. This sets a requirement on average energy deviation of the electron beam to be around $0.3\text{-}0.5 \cdot 10^{-3}$.

I.A.5.5 Cooling optimization

Major parameters which affect beam cooling are:

1. Length of cooling section – directly impacts cooling speed.
2. Cooling current – directly impacts cooling speed.
3. Dependence on beta-function in the cooling solenoid – partially offset by ion beam size increase – corresponding increase of electron beam size leads to reduction of electron density.
4. Alignment of electron-ion beam.
5. Transverse and longitudinal rms velocity spread within electron beam.

For the charge of the electron beam other than 5nC as well as β^* other than 50cm the length of the store is also optimized

I.A.5.6 Cooling performance with and without recombination suppression

The undesired beam loss due to recombination can be controlled by an undulator field in the cooling section. However, the resulting friction force with the undulator field is reduced, which was confirmed by the simulations (see Section I.A.2.4). As a result, depending on the parameters of the electron beam and the cooler, there may be even a small loss in the integrated luminosity with the undulator field being switched on compared to the case with the undulator switched off. For the present baseline parameters in Table I.A.5.1, the integrated average luminosity is higher with the undulator switched on. This is shown in Figs. I.A.5.6-8.

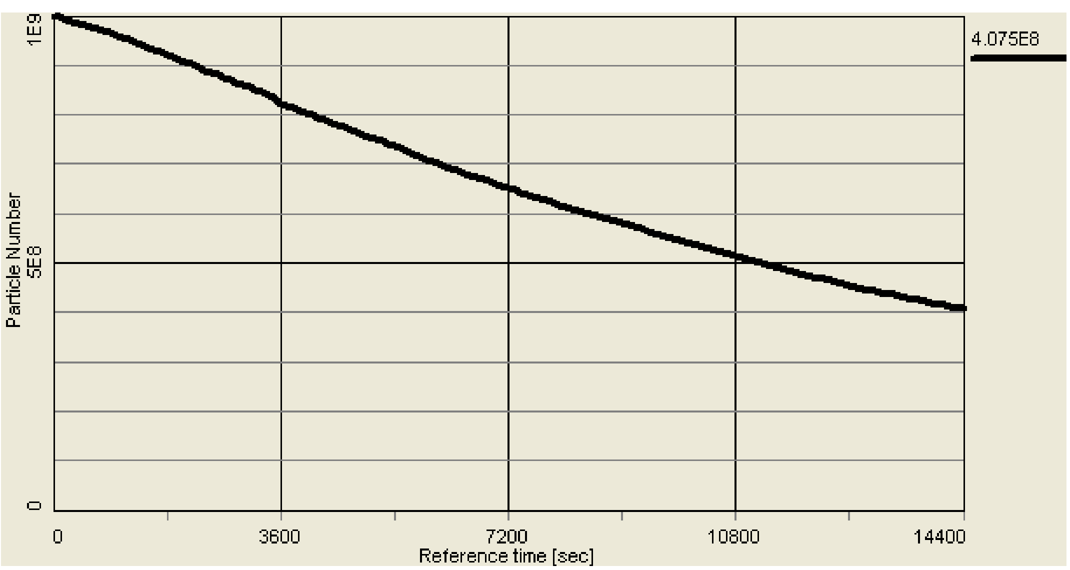

Fig. I.A.5.6 Particle loss only due to collisions in 3 IP (recombination loss is turned off).

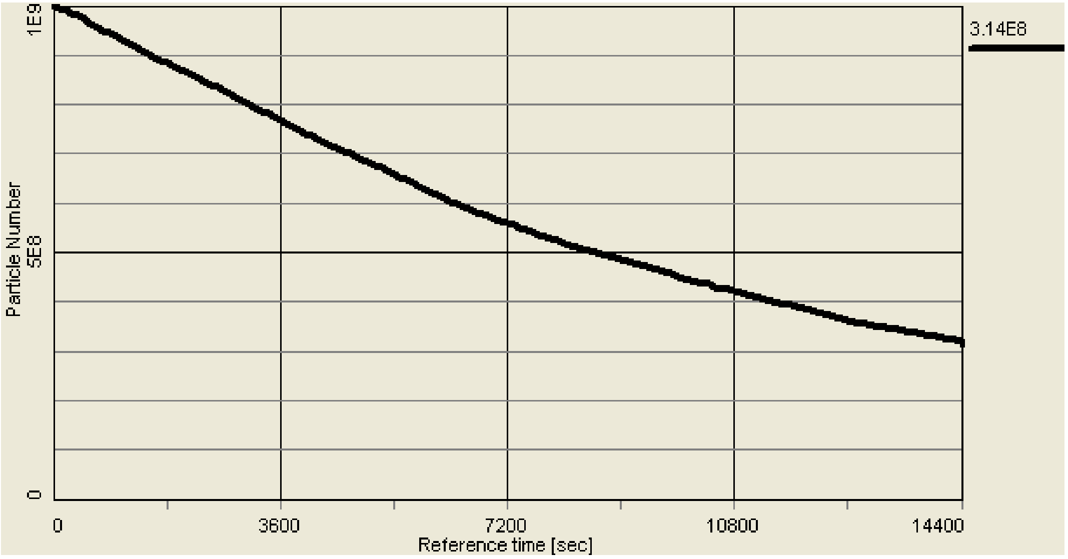

Fig. I.A.5.7 Particle loss due to collisions in 3 IP and recombination in the cooler.

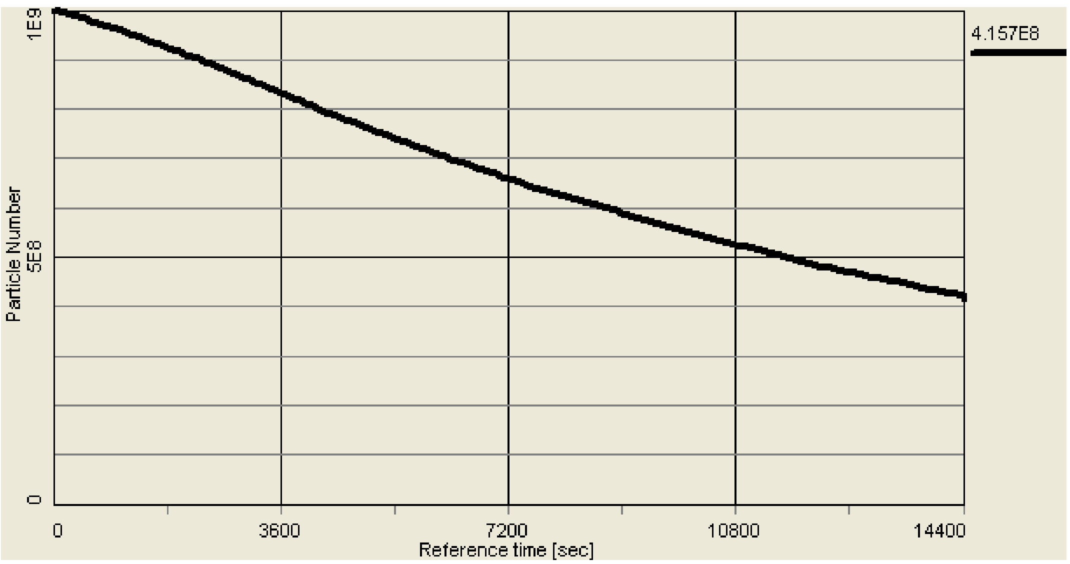

Fig. I.A.5.8 Particle loss due to collisions in 3 IP, recombination in the cooler, and undulator with parameters in Table I.A.4.1.

For parameters in Table I.A.5.1, as a result of loss on recombination, an average luminosity during 4-hour store is $\langle L\rangle = 6\cdot10^{27}$ [$cm^2 sec^{-1}$]. With a suppressed recombination (Fig. I.A.5.8), an average luminosity during 4-hour store becomes $\langle L\rangle = 7\cdot10^{27}$ [$cm^2 sec^{-1}$].

I.A.6 Scenarios of cooling at RHIC: heavy ions

There are various possibilities of using electron cooling at RHIC [6]. Direct cooling at 100 GeV is considered as a base line approach for RHIC-II. However, for eRHIC [29], it is important that cooling is fast enough and sufficient to have the rms beam parameters being cooled substantially, especially the rms bunch length. In such a case, pre-cooling at low energy becomes very attractive due to a strong dependence of the cooling time on energy. For the same reason, cooling is very effective for scenarios with collisions at low energy [6].

Direct cooling of Au ions at storage energy of 100 GeV/n with parameters in Table I.A.5.1 allows us to reach a desired increase in the luminosity for the RHIC-II upgrade.

In addition to the luminosity shown in Figs. I.A.5.1 and I.A.5.5, cooling of the rms transverse emittances and rms bunch length are shown in Figs. I.A.6.1-4. First, one can see, that for present parameters both the rms bunch length and rms emittance are cooled (as shown in Figs. I.A.6.1-2) if the rms dynamics approach is used. Then, using the "Modeled beam" approach (which tracks evolution of beam distribution) in Figs. I.A.6.3-4, one can see that an rms bunch length is actually increasing, this is due to particles at large amplitudes which are not effectively cooled but which are used in the calculation of the rms parameters of the distribution (see Fig. I.A.6.5-8). This effect is especially pronounced in the longitudinal direction since we presently use an rms bunch length of the electron beam equal to 1cm while an rms bunch length of the ion beam is around 20cm.

Difference in the ion rms bunch length resulting due to cooling by using the electron bunch with the rms length of 1 cm and 15 cm is shown in Figs. I.A.6.5-8.

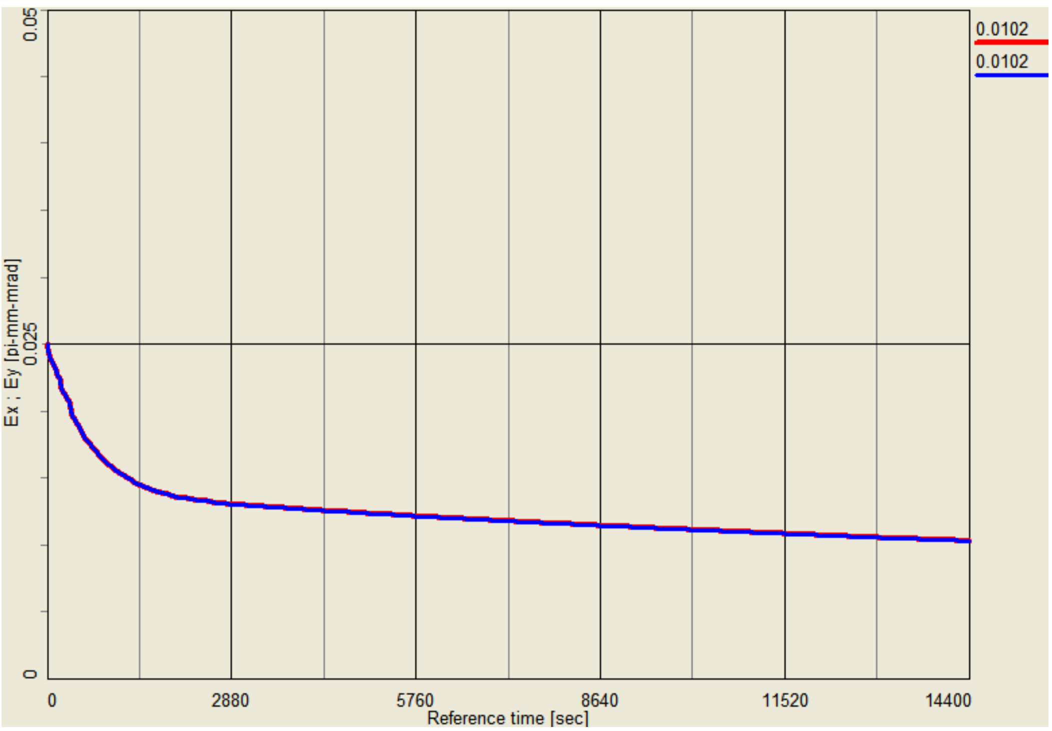

Fig. I.A.6.1 Cooling of horizontal and vertical rms emittances – using "rms dynamics" approach. Plotted emittances are rms unnormalized. Corresponding 95% normalized emittances after 4 hours of cooling are 6.6 π μm.

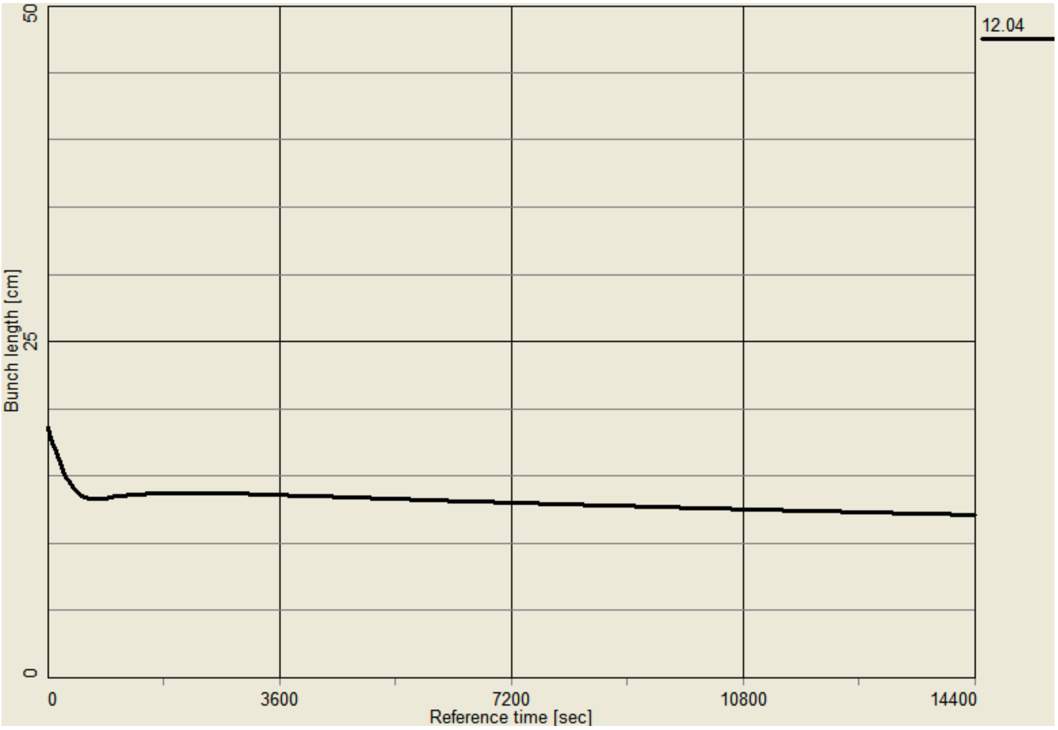

Fig. I.A.6.2 Cooling of rms bunch length – using “rms dynamics” approach, with the ion rms bunch length being cooled to 12 cm.

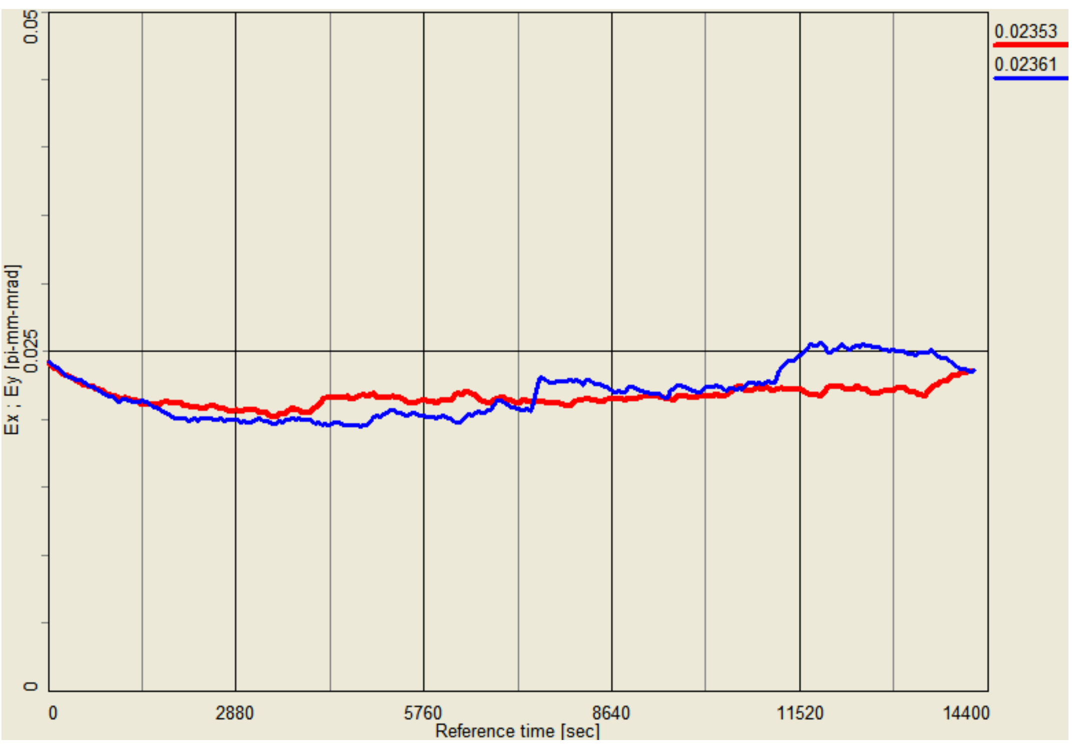

Fig. I.A.6.3 Cooling of horizontal and vertical rms emittances – using “Modeled beam approach”. Plotted emittances are rms unnormalized. Corresponding 95% normalized emittances after 4 hours are 15 π μm.

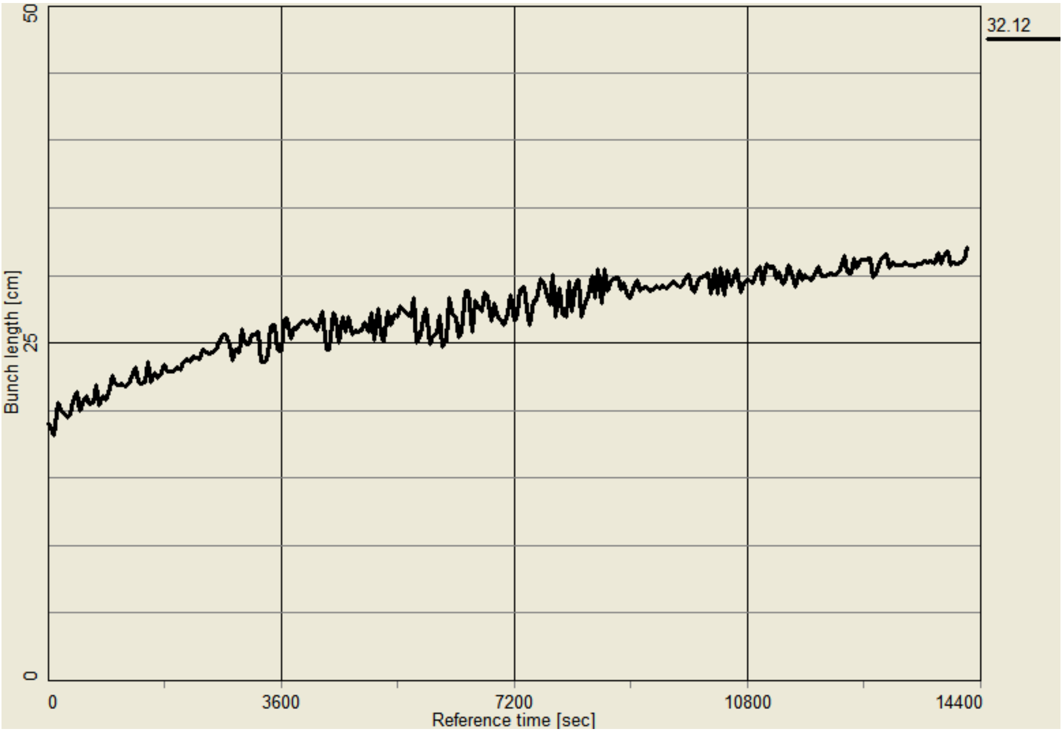

Fig. I.A.6.4 Rms bunch length – using "Modeled beam" approach with 1 cm rms electron bunch. An increase in rms bunch length is due to particles at very large amplitudes.

Figure I.A.6.5 shows 90% bunch length corresponding to Fig. I.A.6.4. One can see that with 1 cm electron bunch sitting in the center of the ion bunch, the 90% bunch length is still increasing. Figure I.A.6.6 shows that more than 10% of the beam in the longitudinal direction is not cooled.

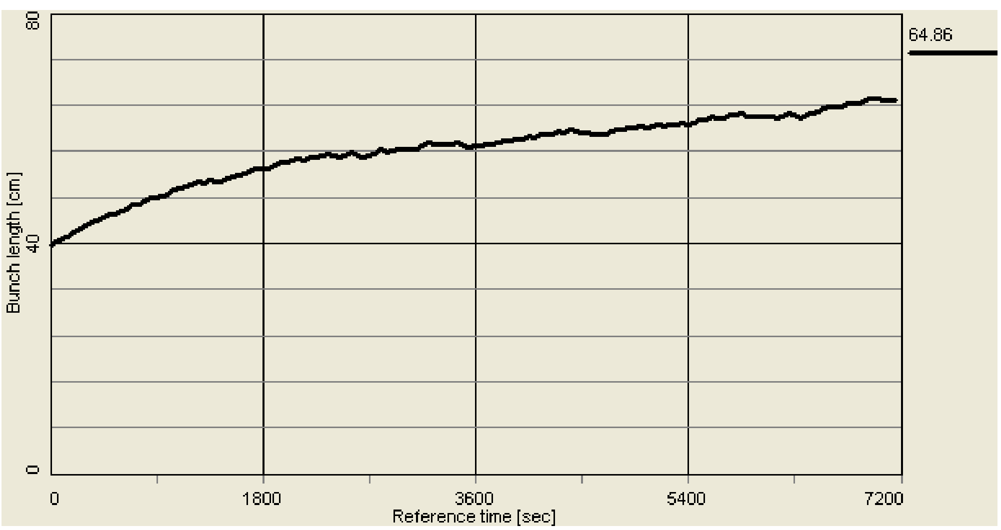

Fig. I.A.6.5 "Modeled beam" approach – 90% bunch length using electron bunch with the rms bunch length of 1 cm.

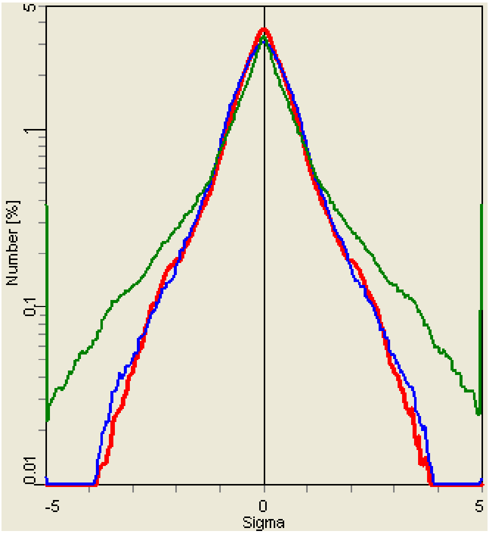

Fig. I.A.6.6 Beam profiles (horizontal: red, vertical: blue, longitudinal: green) after 2 hours of cooling with 1 cm electron rms bunch length.

On the other hand, Fig. I.A.6.7 shows that 90% bunch length is cooled when the electron bunch length is 15 cm rms. Figure I.A.6.8 shows that only 2% of the beam in the longitudinal direction is not cooled in this case.

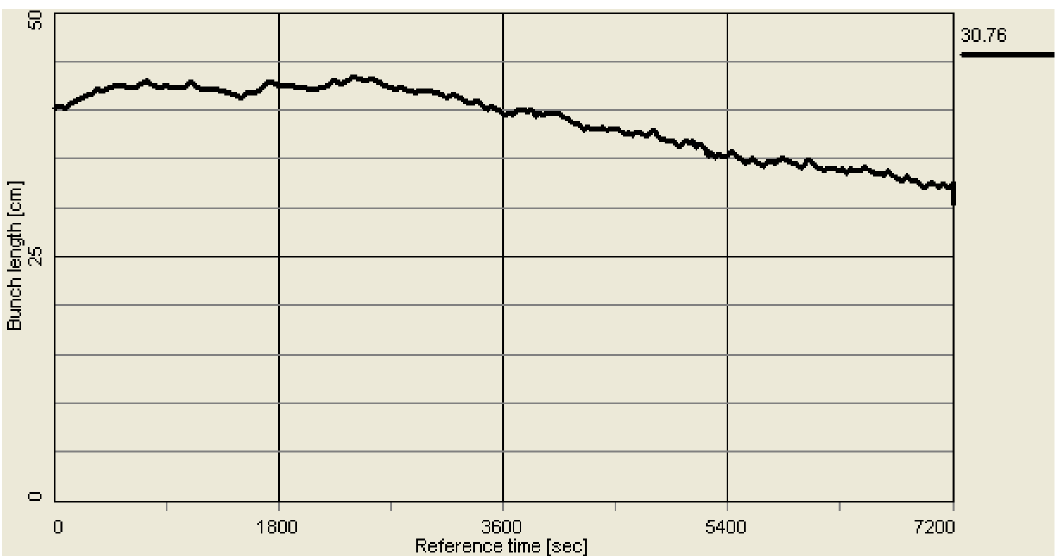

Fig. I.A.6.7 "Modeled beam" approach – 90% bunch length using electron bunch with the rms bunch length of 15 cm.

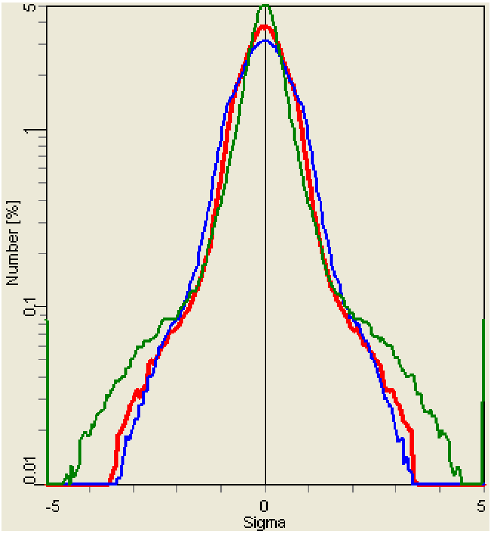

Fig. I.A.6.8 Beam profiles (horizontal: red, vertical: blue, longitudinal: green) after 2 hours of cooling with 15 cm electron rms bunch length.

Several approaches which would help to cool such halo particles are being considered, including painting in the longitudinal direction. In addition, the stochastic cooling system which is presently under development for RHIC should be very effective in cooling of such halo particles. Otherwise, the electron bunch can be stretched to overlap the ion bunch, which is also under discussion.

Painting with the electron beam allows to avoid additional complication in the electron beam transport system. Such a procedure was tested within the BETACOOL code where the electron bunch was moved slowly from the longitudinal center of the ion bunch to 2 rms values in the longitudinal direction and back to the center. The resulting longitudinal distribution (green) can be seen in Figs. I.A.6.9 –I.A.6.12. Cooling of the longitudinal tails and stabilization of the ion rms bunch length was clearly observed. Figures I.A.6.13 –I.A.6.14 show resulting rms bunch length and emittance, respectively. Details of this approach are presently under development.

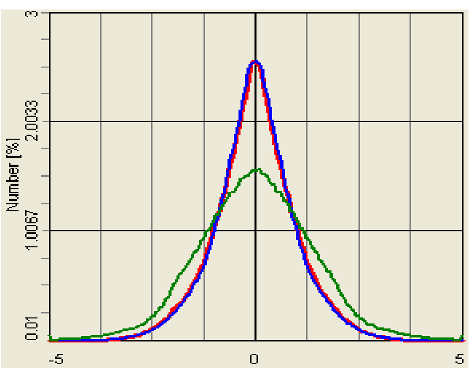

Fig. I.A.6.9 Beam profiles with electron bunch moving towards large amplitudes.

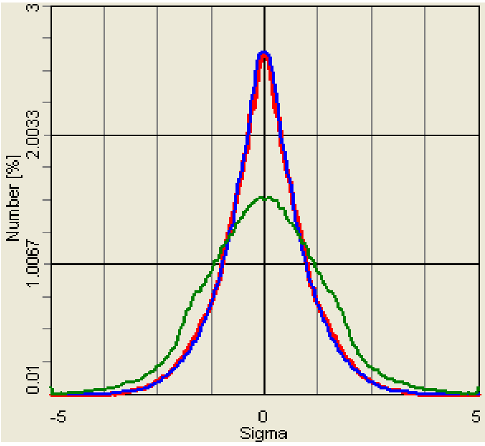

Fig. I.A.6.10 Beam profiles with the electron bunch sitting at 2 rms of the distribution.

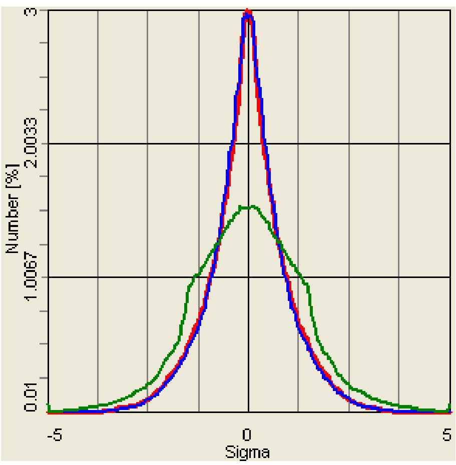

Fig. I.A.6.11 Beam profiles with the electron bunch moving back towards the center.

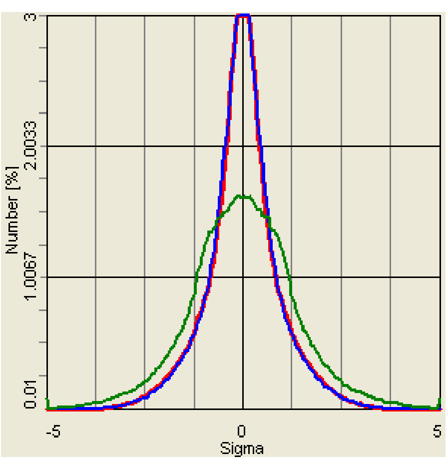

Fig. I.A.6.12 Example of the distribution resulting due to the longitudinal painting.

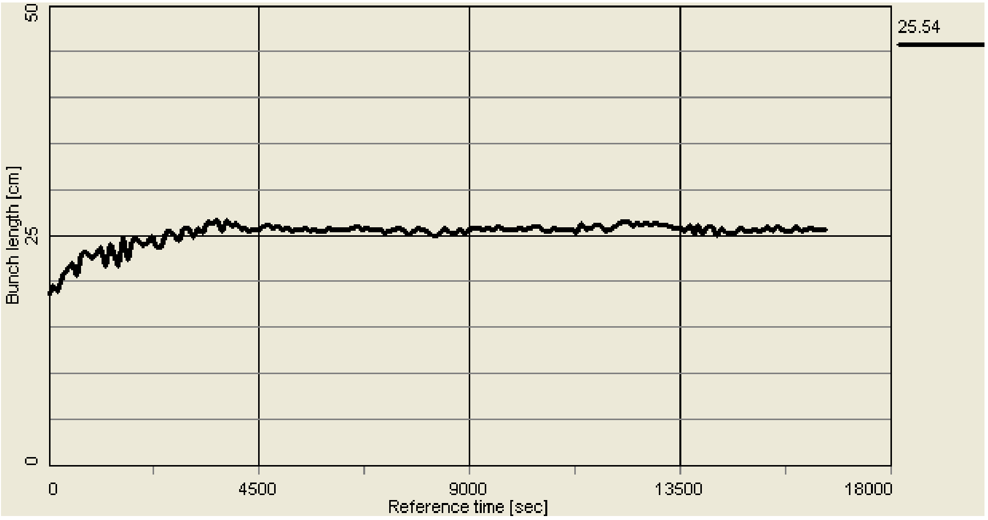

Fig. I.A.6.13 Rms bunch length with painting.

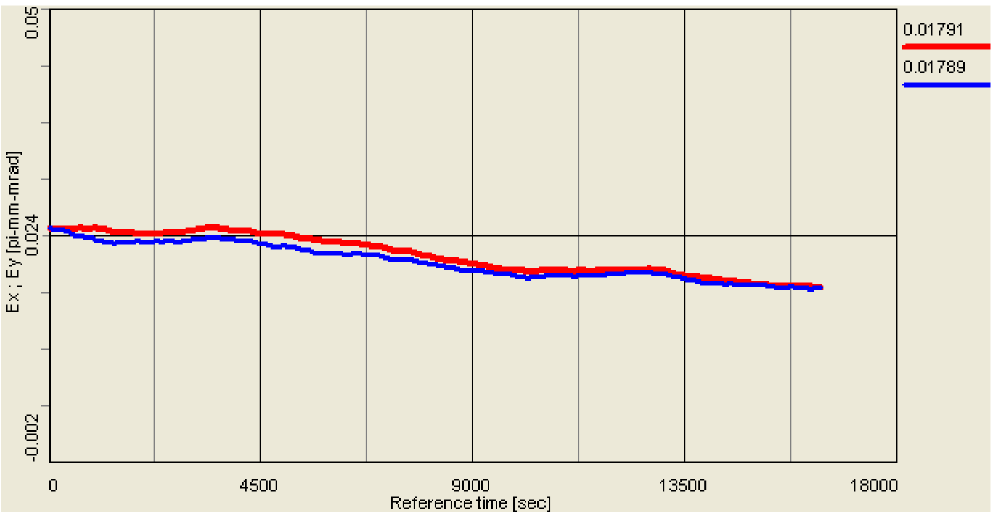

Fig. I.A.6.14 Rms emittance with painting.

With a smooth procedure for painting one can prevent any growth of the rms bunch length, as shown in Fig. I.A.6.15.

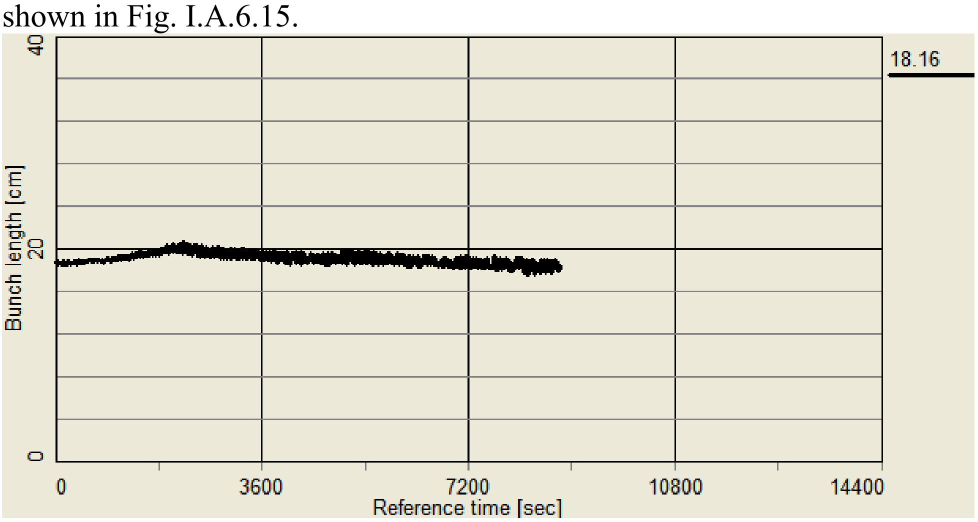

Fig. I.A.6.15 Rms bunch length with painting.

I.A.7 Scenarios of cooling at RHIC: protons

For protons, the best performance is achieved when protons are first pre-cooled at low energy and cooling is continued either at beam energy of 110 GeV or 250 GeV. Various scenarios for cooling of protons were performed (not discussed here). Here, we just give two examples of cooling at 110 and 250 GeV.

For the case of 110 GeV, even without pre-cooling at low energy one obtains promising results. Such a direct cooling at 110 GeV is shown in Figs. I.A.7.1-2 for the rms emittance and bunch length, respectively. The following parameters were used. Protons: initial 95% normalized emittance 20 π μm, rms radius 4.7mm (beta function 800m), h=360, Urf=300kV. Electrons: q=5nC, rms emittance 4 π μm , rms radius 4.8mm, rms bunch length 1 cm.

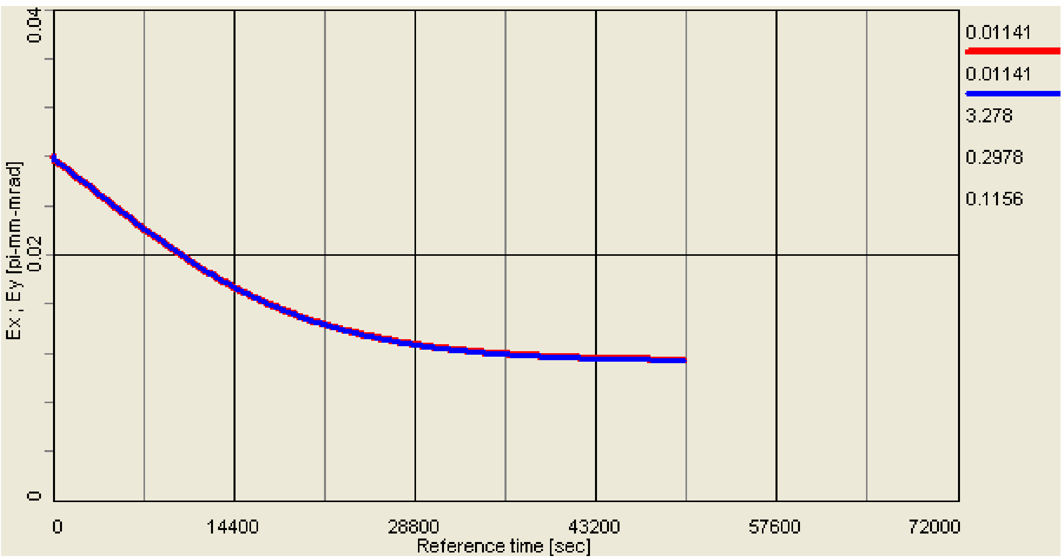

Fig. I.A.7.1 Time evolution of horizontal and vertical rms emittances - direct cooling of protons at 110 GeV. Plotted emittances are rms unnormalized.

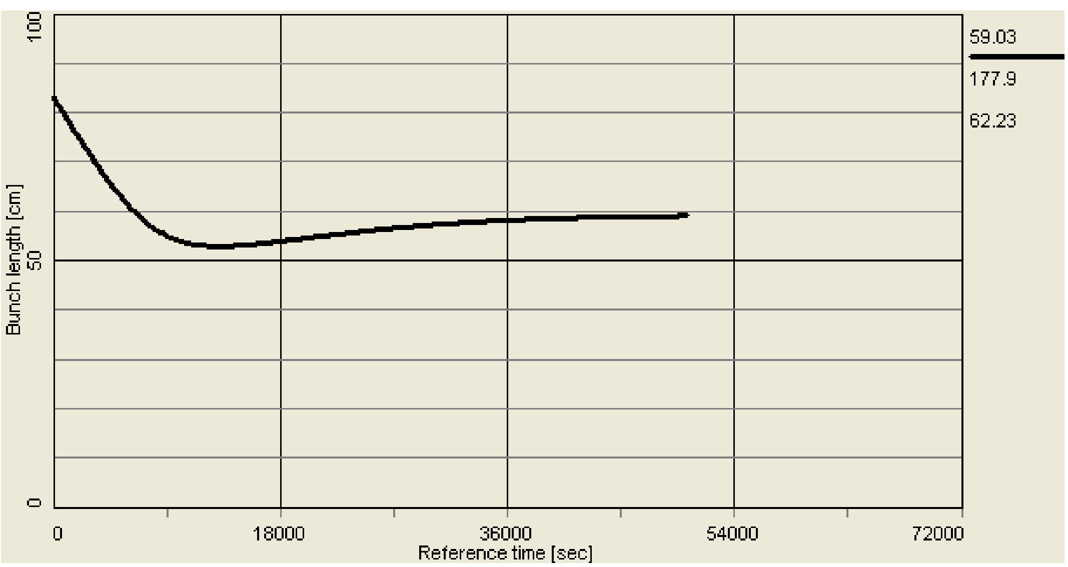

Fig. I.A.7.2 Time evolution of rms bunch length – direct cooling at 110 GeV.

For the case of 250GeV, cooling is shown in Figs. I.A.7.3-4 for the rms emittance and bunch length, respectively. The following parameters were used. Protons: initial 95% normalized emittance 12 π μm (beta function 800m), h=2520, Urf=800kV, initial rms bunch length 29cm. Electrons: q=5nC, rms emittance 2 π μm , rms bunch length 1 cm.

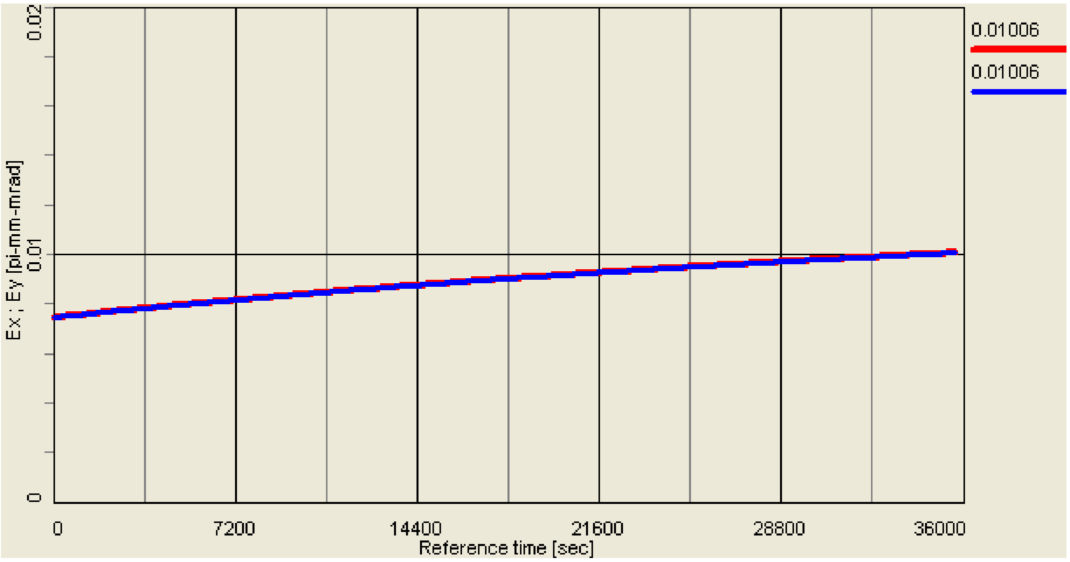

Fig. I.A.7.3 Time evolution of horizontal and vertical rms emittances - cooling of protons at 250 GeV. Plotted emittances are rms unnormalized.

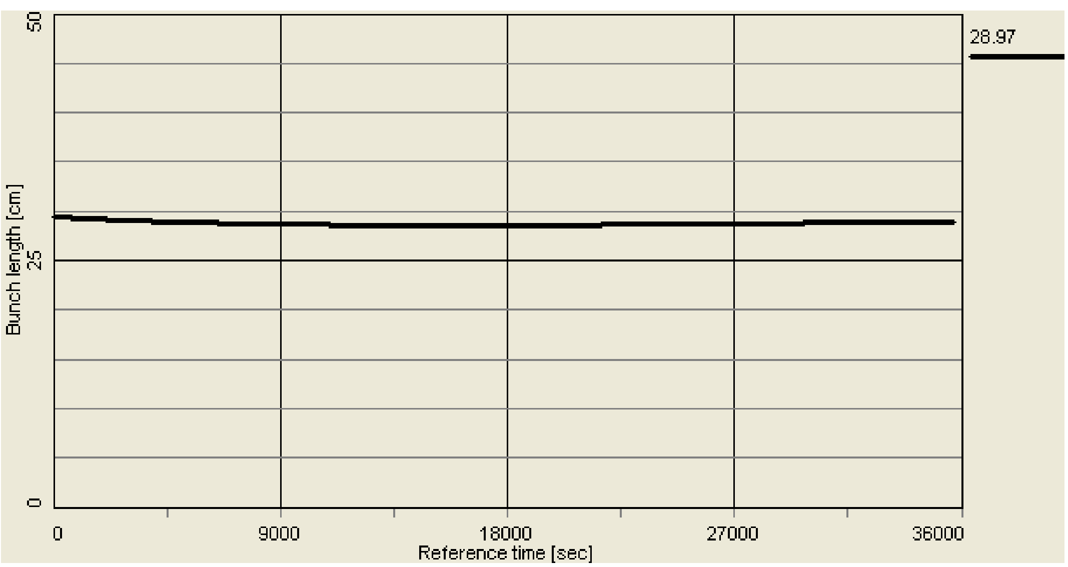

Fig. I.A.7.4 Time evolution of rms bunch length – cooling at 250 GeV.

Figures I.A.7.3-4 show that the rms bunch length can be kept within the bucket acceptance of 30 cm rms, while the growth of rms emittance is marginal.

I.A.8 Luminosity limitations under cooling

I.A.8.1 Incoherent beam-beam effects

The electro-magnetic force field of a moving bunch produces a force which acts on individual particles in another bunch moving in the opposite direction. Such a force acting on individual particles is referred to as incoherent beam-beam force. One can integrate this force over the collision to obtain the incoherent beam-beam kick.

Beam-beam kick for head-on collision

One typically starts consideration of beam-beam effects with calculation of an increment of transverse particle momentum change after crossing the encounter bunch, considering "strong-weak" approximation of beam-beam interaction [30]. In this model it is assumed that particles of the weak-beam (index 2) are influenced by a strong electromagnetic field of the opposite bunch (index 1), while the strong bunch does not feel any field of the weak bunch. Assume that opposite bunch with N_1 particles has the Gaussian space charge density distribution with r.m.s. bunch size σ_x, σ_z, σ_s:

$$\rho(x,z,s,v_1,t)=\frac{q_1N_1}{(2\pi)^{3/2}\sigma_x\sigma_y\sigma_z}\exp\left(-\frac{x^2}{2\sigma_x^2}-\frac{z^2}{2\sigma_{zy}^2}-\frac{(s-v_1t)^2}{2\sigma_{sz}^2}\right). \qquad \text{(I.A.8.1)}$$

where $V_1=\beta\cdot c$ is the average velocity of the strong beam particles. In the reference frame moving with V_1 velocity (noted as prime coordinate system), the longitudinal position of a weak beam particle is :

$$s'=\gamma(s-v_1t). \qquad \text{(I.A.8.2)}$$

Similarly, the strong beam density distribution is

$$\rho'(x,z,s')=\frac{N_1}{(2\pi)^{3/2}\sigma_x\sigma_z(\sigma_s\gamma)}\exp\left(-\frac{x^2}{2\sigma_x^2}-\frac{z^2}{2\sigma_z^2}-\frac{s'^2}{2\sigma_s^2\gamma^2}\right). \qquad \text{(I.A.8.3)}$$

Electrostatic potential of the Gaussian bunch is [31, 32]:

$$U'(x,z,s')=\frac{q_1N_1}{4\pi^{3/2}\varepsilon_0}\int_0^\infty\frac{\exp\left[-\frac{x^2}{(2\sigma_x^2+w)}-\frac{z^2}{(2\sigma_z^2+w)}-\frac{s'^2}{(2\sigma_s^2\gamma^2+w)}\right]}{\sqrt{(2\sigma_x^2+w)(2\sigma_z^2+w)(2\sigma_s^2\gamma^2+w)}}dw, \qquad \text{(I.A.8.4)}$$

where q_1 is the electric charge of the "1" particle, gives us the transversal components of electrostatic field in the moving reference frame: differentiation of the potential (I.A.8.4) $E'_x=-\partial U'/\partial x$, $E'_z=-\partial U'/\partial z$:

$$E_x = -\frac{q_1 N_1 \gamma}{2\pi^{3/2}\varepsilon_0}\int_0^\infty \frac{\exp\left[-\frac{x^2}{(2\sigma_x^2+w)}-\frac{z^2}{(2\sigma_z^2+w)}-\frac{\gamma^2(s-v_1t)^2}{(2\sigma_s^2\gamma^2+w)}\right]}{(2\sigma_x^2+w)^{3/2}\sqrt{(2\sigma_z^2+w)}\sqrt{(2\sigma_s^2\gamma^2+w)}}dw\ , \qquad \text{(I.A.8.5)}$$

with analogous expression for E_z component. Moving bunch of charged particles creates magnetic field:

$$B_x = -\beta_1\frac{E_z}{c}\ ,\ B_z = -\beta_1\frac{E_x}{c} \qquad \text{(I.A.8.6)}$$

The equations of the test particle transverse motion are

$$\frac{dp_x}{dt} = q_2[E_x - (-v_2B_z)] = q_2E_x(1+\beta_1\beta_2),$$
$$\frac{dp_z}{dt} = q_2[E_z - (-v_2B_x)] = q_2E_z(1+\beta_1\beta_2). \qquad \text{(I.A.8.7)}$$

To define a change of particle momentum after crossing the encounter bunch, the equations (I.A.8.7) have to be integrated along the time of interaction. Assuming that particle position and Lorentz force are not changed during test particle crossing the encounter bunch (thin lens approximation) one gets

$$\Delta p_x = q_2(1+\beta_1\beta_2)\int_{-\infty}^{\infty}E_xdt = -\frac{q_1q_2N_1(1+\beta_1\beta_2)}{2\pi^{3/2}\varepsilon_0(v_2-v_2)}x\int_0^\infty\frac{\exp\left[-\frac{x^2}{(2\sigma_x^2+w)}-\frac{z^2}{(2\sigma_z^2+w)}\right]}{(2\sigma_x^2+w)^{3/2}\sqrt{(2\sigma_z^2+w)}}dw, \quad \text{(I.A.8.8)}$$

and similar for Δp_z.

In the linear approximation, the integral in Eq. (I.A.8.8) can be evaluated analytically:

$$\int_0^\infty\frac{\exp\left[-\frac{x^2}{(2\sigma_x^2+w)}-\frac{z^2}{(2\sigma_z^2+w)}\right]}{(2\sigma_x^2+w)^{3/2}\sqrt{(2\sigma_z^2+w)}}dw \approx \int_0^\infty\frac{dw}{(2\sigma_x^2+w)^{3/2}\sqrt{(2\sigma_z^2+w)}} = \frac{1}{\sigma_x(\sigma_x+\sigma_z)}, \quad \text{(I.A.8.9)}$$

which gives:

$$\Delta p_x = -\frac{q_1q_2N_1(1+\beta_1\beta_2)}{2\pi\varepsilon_0(\beta_2+\beta_1)\sigma_x(\sigma_x+\sigma_z)}x\,. \qquad \text{(I.A.8.10)}$$

Let us introduce the value of beta-function at the interaction point β_x^*, β_z^*. Then the change of slope of particle trajectory in linear approximation can be written as follows:

$$\Delta\frac{dx}{ds}=\frac{\Delta p_x}{p_s}=4\pi\frac{\xi_x}{\beta_x^*}x\,,\ \Delta\frac{dz}{ds}=\frac{\Delta p_z}{p_s}=4\pi\frac{\xi_z}{\beta_z^*}z\,, \qquad \text{(I.A.8.11)}$$

where ξ_x, ξ_z are beam-beam parameters, which have a meaning of linear part of betatron tune shift due to beam-beam collision [30]:

$$\xi_x=N_1\frac{\beta_x^*}{4\pi}\frac{q_1q_2}{4\pi\varepsilon_0 m_2c^2}\frac{(1+\beta_1\beta_2)}{\gamma_2\beta_2(\beta_1+\beta_2)}\frac{2}{\sigma_x(\sigma_x+\sigma_z)}, \qquad \text{(I.A.8.12)}$$

$$\xi_z=N_1\frac{\beta_y^*}{4\pi}\frac{q_1q_2}{4\pi\varepsilon_0 m_2c^2}\frac{(1+\beta_1\beta_2)}{\gamma_2\beta_2(\beta_1+\beta_2)}\frac{2}{\sigma_z(\sigma_x+\sigma_z)}. \qquad \text{(I.A.8.13)}$$

For collisions of the particles at equal velocities ($\beta_1 = \beta_2 = \beta$), charge numbers ($q_1 = q_2 = Z$) and atomic numbers the beam-beam parameters can be simplified:

$$\xi_x=\frac{\beta^*}{4\pi}\frac{Z^2}{A}r_p\frac{N(1+\beta^2)}{\beta^2\gamma\sigma_x(\sigma_x+\sigma_z)}, \qquad \text{(I.A.8.14)}$$

$$\xi_z=\frac{\beta^*}{4\pi}\frac{Z^2}{A}r_p\frac{N(1+\beta^2)}{\beta^2\gamma\sigma_z(\sigma_x+\sigma_z)}. \qquad \text{(I.A.8.15)}$$

For the relativistic factor β=1 one has

$$\xi=\frac{\beta^*}{2\pi}\frac{Z^2}{A}r_p\frac{N}{\gamma\sigma_z(\sigma_x+\sigma_z)} \qquad \text{(I.A.8.16)}$$

Stability of linear incoherent motion

In the linear approximation, the motion of a test particle in the presence of the other beam is stable if the absolute value of the trace of the one-turn transfer matrix is less than 2.

Such stability criteria gives very large attainable linear beam-beam tune shifts, which indicates that much smaller experimentally achieved beam-beam parameters are not due to this stability mechanism.

I.A.8.2 Coherent beam-beam effects

Coherent beam-beam effects arise from the forces which an exciting bunch exerts on a whole test bunch during collision. The corresponding coherent kick is obtained by integrating incoherent beam-beam kick over the charge distribution of the test bunch. In ideal case, due to a symmetry, the coherent beam-beam kick vanishes for head-on collisions.

Linear tune shift

The linear coherent beam-beam tune shift can be calculated and becomes just one half of the linear incoherent shift ξ :

$$\Xi = \frac{\beta^*}{4\pi}\frac{Z^2}{A} r_p \frac{N}{\gamma\sigma_x\left(\sigma_x + \sigma_z\right)} \tag{I.A.8.17}$$

Stability of linear coherent motion

Coherent oscillation of two beam under certain condition can lead to an instability. With one bunch per beam to modes are possible, the 0-mode, where both beam oscillate in phase and π-mode where both beam oscillate out of phase. With *m* bunches per beam, one gets 2*m* modes of oscillation, correspondingly.

The stability of the system can be also calculated in the linear matrix theory. Although the threshold is now significantly lower then in the incoherent case it is still well above the experimentally observed beam-beam limits.

I.A.8.3 Nonlinear effects and beam-beam limit

Non-linear tune spread and resonances

The nonlinear variation of the beam-beam force with radius in a round Gaussian beam causes a tune shift of individual particles to have dependence on particle oscillation amplitude. For the distribution of particles within the beam this results in a tune-spread in the beam. In addition the beam-beam force drives non-linear resonances.

Experimental beam-beam limit is usually attributed to excitation of non-linear resonances. Overlapping of resonances results in stochastic particles motion with corresponding particle loss. The strength of nonlinear beam-beam resonances can be related to the incoherent beam-beam parameter which allows to use its value to describe beam-beam limit. In principle, an estimate of the real beam-beam limit should include nonlinear resonances excited by the magnet imperfections which then makes beam-beam limit to be machine dependent.

In lepton machines, the beam-beam tune spread is much high than in hadron machine. As a result, many nonlinear resonances are crossed. However, diffusion caused by a very high-order nonlinear resonance is compensated by intrinsic damping mechanism of lepton machines which is the synchrotron radiation.

In the absence of damping mechanism diffusion even by a very high-order resonances can have significant effect on particles losses, which is believed to be the case for hadron machine. Introduction of additional fast damping mechanism, such as e-cooling can offset diffusion due to high-order resonance, at least partially, and thus lead to higher values of beam-beam parameters. Due to a very slow cooling rates at high energy, this damping mechanism may not lead to compensation of beam-beam diffusion. However, this question of equilibrium between beam-beam and cooling requires very careful computational study, especially for non-Gaussian distributions which may appear as a result of cooling.

I.A.8.4 Beam-beam simulations for ion beam under cooling

It is extremely important to treat beam-beam effects for the ion beam while the cooling is present. The main purpose of cooling is to counteract diffusion of ion beam which may be caused by various effects. For accurate treatment, dynamic simulation code should include both cooling and diffusion sources, including intrabeam scattering and beam-beam diffusion. As a simple model, one can describe beam-beam effects with a diffusion coefficient, based on beam-beam space-charge force. Such a coefficient, either approximate analytic or empiric (based on real measurements in RHIC) can be used in dynamic simulation code. Simulations of beam cooling including beam-beam diffusion are planned in the future.
As a result of beam-beam force one has two major effects: excitation of beam-beam resonances and tune spread. Because of the tune spread many non-linear imperfection resonances can be crossed which results in a significant beam diffusion and in so called empiric beam-beam limit. A reliable way to account for beam-beam effects and to have a reasonable description of achievable beam-beam limit is to include non-linear optics of the machine (imperfection resonance) into account. Such simulations of beam-beam effects and cooling are planned in the framework of UAL simulation [33]. In addition, the UAL based simulation should describe both incoherent and coherent effects in a self-consistent manner.

Presently, simulations of electron cooling are done without taking into account beam-beam diffusions. As a guideline we only use the values of the beam-beam parameter which is calculated from the local density when the "Model beam" approach is being used.

As an example, Figs. I.A.8.1 and I.A.8.2 show the beam-beam parameter for the cooling simulations in Fig. I.A.5.1 and parameters in Table I.A.5.1, using the "rms dynamics" and "Model beam" approach, respectively.

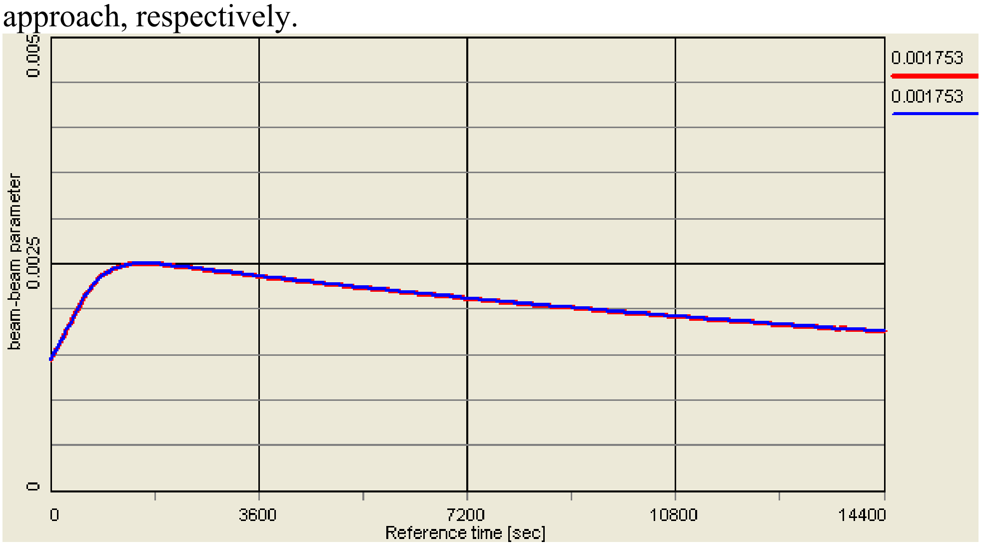

Fig. I.A.8.1 Resulting beam-beam parameter for parameters in Table I.A.5.1, calculated using rms dynamics approach.

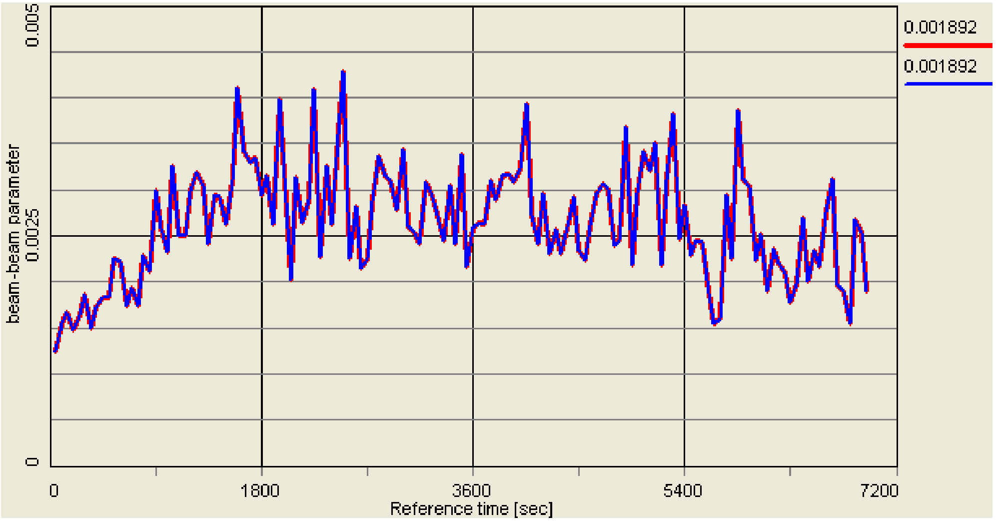

Fig. I.A.8.2 Resulting beam-beam parameter for parameters in Table I.A.5.1, calculated via local density using “Model beam” approach (oscillations are due to the numerical noise).

I.A.9 Effects on electron beam

For RHIC one needs to cool ion beam in two rings (yellow and blue). The present approach is to use a single ERL and the same electron beam to cool the ion bunch in both rings. To ensure good cooling performance a quality of the electron beam should not suffer significantly as a result of the electron beam transport, merging of the electron and ion beam, the interactions with the ion beam.

An increase in the electron emittance and momentum spread was estimated for the following effects: intra-beam scattering within the electron beam, Coherent Synchrotron Radiation (CSR) radiation and intra-beam scattering between the electron and ion beam. The largest effect was found to be electron-ion IBS. But even this effect results in only about 1% increase in the rms momentum spread of the electron beam which is negligible. A possible energy loss due to CSR (on the level of 10^{-3}) may need to be corrected by an extra cavity.

Another approach which is being considered is to adjust timing and return path of the electron beam in such a way that each electron bunch is used only once for the interaction with the ion bunch.

I.A.10 Effects of electron beam on ion beam dynamics

I.A.10.1 Coherent ion-electron interactions

A simple description of such interaction can be done via the model of two oscillators [34]. Even with such simple model one can obtain that for a very high electron densities and long cooling section the net effect of ion-electron interaction can result in “heating” of the ion beam rather than cooling.

An approximate models were developed in Refs. [34, 35, 36] which allow us to estimate thresholds of this type of instabilities for RHIC parameters. Such an estimate for the RHIC cooler showed that, for proposed density of the electron beam, the ion beam will remain stable both in the transverse and longitudinal directions [37].

I.A.10.2 Collective instabilities for ion distribution under cooling

A careful study of collective instabilities becomes a critical issues for ion beam under cooling at least for two reason:

- tune spread and momentum spread decreases which may result in unsufficient Landau damping

- direct space-charge field increases as the beam cools down with a formation of dense core.

Requirements on coupling impedance after cooling

For the longitudinal stability a rough condition is

$$\left|\frac{Z}{n}\right| \le F_L \frac{A}{Z_i^2} \frac{\beta^2\gamma\left(m_p c^2/e\right)|\eta|}{I_0}\left(\frac{\Delta p}{p}\right)^2_{FWHM} \qquad \text{(I.A.10.1)}$$

where the longitudinal form factor depends on the distribution and approximately F_L=1. Here, I_0 is the average ion beam current for a coasting beam. For a bunched beam, one can roughly use the local peak current $I_p = eZ_i\beta c/l_b$.

For low-energy cooling, cooling above transition becomes a problem due to the space-charge contribution to the impedance which results in a significant tune shift. For RHIC energies, the space-charge impedance in negligible so that stability will be simply governed by a degree of a collapse of momentum spread Δp/p. The process of cooling should be carefully controlled to avoid large decrease in Δp/p.

For the transverse stability, the requirement on the transverse impedance is given by

$$Z_t \le 4F_T \frac{A}{Z_i^2}\frac{\gamma\left(mc^2/e\right)}{I_0}\frac{Q}{R}\left(\Delta Q\right)_{FWHM} \qquad \text{(I.A.10.2)}$$

where full tune-spread ΔQ_{FWHM} is given by

$$\left(\Delta Q\right)_{FWHM} = \left[\left(\left|(n-Q)\eta + Q'\right|(\Delta p/p)\right)^2 + \left(\left(\partial^2 Q/\partial a^2\right)a^2\right)^2\right]^{1/2} \qquad \text{(I.A.10.3)}$$

The first term in Eq. (I.A.10.3) is due to the revolution frequency, the second term is due chromaticity Q' and the third term is due to the nonlinear tune spread with octupoles.

A study of the longitudinal and transverse stability of cooled ion beam in RHIC, with the beam distribution resulting due to cooling will be done in the future.

I.A.11 REFERENCES

[1] A.O. Sidorin et al., Nuclear Instr. Methods A 558, p. 325, 2006 (Joint Institute for Nuclear Research, Dubna, Russia http://lepta.jinr.ru).
[2] C. Nieter, J. Cary, J. Comp. Phys. 196 , p.448 (2004).
[3] S. Nagaitsev et al., PRL 96, 044801 (2006).
[4] I. Ben-Zvi and V. Parkhomchuk, Tech. Report C-AD/AP/47 (2001).
[5] V.V. Parkhomchuk, A.N. Skrinky, Rep. Prog. Physics 54, p.919 (1991).
[6] A.V. Fedotov et al., Proceedings of PAC05, p 4236; p.4251 (2005).
[7] I. Ben-Zvi, AIP Con. Proceedings 821 (COOL05, Galena, IL), p.75 (2005).
[8] Ya. Derbenev, TJAB Note, February 2001 (unpublished).
[9] V. Litvinenko, independently proposed to use undulator for recombination suppression.
[10] S. Chandrasekhar, *Principles of Stellar Dynamics* (U. Chicago Press, 1942).
[11] Ya. Derbenev, A. Skrinsky, Part. Accelerators 8, p. 235 (1978).
[12] J. J. Binney, MNRAS 181, p. 735 (1977).
[13] D.L. Bruhwiler *et al*., AIP Conf. Proceed. **773** (Bensheim, Germany, 2004), p. 394.
[14] A. Fedotov, D. Bruhwiler, D. Abell A. Sidorin., AIP Conf. Proc. 821, p. 319 (2005).
[15] A.V. Fedotov et al., submitted to PRST (2006)..
[16] L. Prost et al., to be presented at HB2006 (Tsukuba, Japan).
[17] D. Abell et al., to be presented at HB2006 (Tsukuba, Japan).
[18] A. Piwinski, Proc. of 9th Intern. Conf. High Energy Acc. (1974); CERN 92-01, p. 405.
[19] M. Martini, CERN PS/84-9 (AA), 1984.
[20] J. Bjorken and S. Mtingwa, Particle Accel. 13 (1983), p.115.
[21] V. Lebedev, AIP Conf. Proc. 773 (HB2004), p. 440.
[22] W. Fischer et al. Proccedings of EPAC02, p. 236 (2002).
[23] J. Wei et al., AIP Conf. Proc. 773 (HB2004), p. 389.
[24] A. Fedotov et al, unpublished (2004).
[25] A. Fedotov et al, to be presented at HB2006 (Tsukuba, Japan).
[26] A. Burov, "Electron cooling against IBS", FNL-TM-2258 (2003).
[27] A. Fedotov et al., Proceedings of PAC05, p. 4263 (2005).
[28] G. Parzen, Tech. Notes C-AD/AP/144, C-AD/AP/150 (2004).
[29] "eRHIC Zeroth-Order Design Report", BNL C-A/AP Note 142 (2004)
http://www.agsrhichome.bnl.gov/eRHIC/eRHIC_ZDR.htm
[30] T.Katayama et al. MUSES Conceptual Design Report, RIKEN, May 1999.
[31] O.D. Kellogg, Foundations of Potential Theory (Dover, New York, 1953).
[32] K.Takayama, Lettere al Nuovo Cimento, Vol.34, No.7,p.190 (1982).
[33] N. Malitsky, R. Talman, "Unified Accelerator Libraries", AIP 391 (1996).
[34] V.V. Parkhomchuck, V.B. Reva, J. of Exp. and Theor. Physics, V.91, p. 975 (2000).
[35] P.R. Zenkevich, A.E. Bolshakov, NIM A 441, p. 441 (2000).
[36] V.B. Reva (2002).
[37] G. Wang, AIP Conf. Proc. 821 (COOL05, Galena, IL), p. 164 (2005).